

BRNO UNIVERSITY OF TECHNOLOGY

VYSOKÉ UČENÍ TECHNICKÉ V BRNĚ

FACULTY OF ELECTRICAL ENGINEERING AND COMMUNICATION
DEPARTMENT OF RADIO ELECTRONICS

FAKULTA ELEKTROTECHNIKY A KOMUNIKAČNÍCH TECHNOLOGIÍ
ÚSTAV RADIOELEKTRONIKY

SUPPORT SYSTEM FOR ADMINISTRATION AND CONTROL OF FSO
TRANSCEIVER

DIPLOMA THESIS
DIPLOMOVÁ PRÁCE

AUTHOR
AUTOR PRÁCE

Bc. LUKÁŠ JANÍK

BRNO 2016



BRNO UNIVERSITY OF TECHNOLOGY

VYSOKÉ UČENÍ TECHNICKÉ V BRNĚ

FACULTY OF ELECTRICAL ENGINEERING AND COMMUNICATION

FAKULTA ELEKTROTECHNIKY
A KOMUNIKAČNÍCH TECHNOLOGIÍ

DEPARTMENT OF RADIO ELECTRONICS

ÚSTAV RADIOELEKTRONIKY

SUPPORT SYSTEM FOR ADMINISTRATION AND CONTROL OF FSO TRANSCEIVER

PODPŮRNÝ SYSTÉM PRO SPRÁVU A ŘÍZENÍ FSO TRANSCEIVERU

MASTER'S THESIS

DIPLOMOVÁ PRÁCE

AUTHOR

AUTOR PRÁCE

Bc. Lukáš Janík

SUPERVISOR

VEDOUCÍ PRÁCE

prof. Ing. Otakar Wilfert, CSc.

BRNO 2016

Diplomová práce

magisterský navazující studijní obor **Elektronika a sdělovací technika**
Ústav radioelektroniky

Student: Bc. Lukáš Janík

ID: 147650

Ročník: 2

Akademický rok: 2015/16

NÁZEV TÉMATU:

Podpůrný systém pro správu a řízení FSO transceiveru

POKYNY PRO VYPRACOVÁNÍ:

Seznamte se s metodou a modelováním optických bezkabelových spojů. Optická bezkabelová komunikace nabízí řadu výhod oproti radiové komunikaci, avšak kvalita přenosu do značné míry závisí na stavu počasí. Prostudujte základní standardní i nestandardní atmosférické jevy, které zhoršují kvalitu přenosu a vypracujte přehled metod, které se používají na snížení vlivu atmosféry na spoj.

Navrhněte a realizujte funkční vzorek (prototyp) podpůrného systému pro správu modulu FSO přijímače - vysílače. Podpůrný systém je určen k odmlžování a odmrazování optiky a napájení elektrické části transceiveru. Součástí realizace je implementace jednoúčelového dvouportového Ethernetového přepínače, který umožní posílat data pomocí optického bezkabelového mostu a zároveň přistupovat k webovému rozhraní celého zařízení za účelem vizualizace statistik a nastavení parametrů hlavního modulu.

DOPORUČENÁ LITERATURA:

[1] YOUNG, Matt. Optics and Lasers: an engineering physics approach. Berlin: Springer Verlag, 1977, xii, 207 s. Springer series in optical sciences, vol. 5. ISBN 3540081267.

[2] BOUCHET, O. et al. Free-Space Optics. Propagation and Communication. London: ISTE, 2006. ISBN 10: 1-905209-02-9

Termín zadání: 8.2.2016

Termín odevzdání: 19.5.2016

Vedoucí práce: prof. Ing. Otakar Wilfert, CSc.

Konzultant diplomové práce:

doc. Ing. Tomáš Kratochvíl, Ph.D., předseda oborové rady

UPOZORNĚNÍ:

Autor diplomové práce nesmí při vytváření diplomové práce porušit autorská práva třetích osob, zejména nesmí zasahovat nedovoleným způsobem do cizích autorských práv osobnostních a musí si být plně vědom následků porušení ustanovení § 11 a následujících autorského zákona č. 121/2000 Sb., včetně možných trestněprávních důsledků vyplývajících z ustanovení části druhé, hlavy VI. díl 4 Trestního zákoníku č.40/2009 Sb.

ABSTRACT

This thesis deals with problematics of free space optical links (FSO). The first chapter discusses common benefits, essential principles and key components of a FSO link. The second chapter deals with an atmosphere in terms of beam propagation, its composition, common variables and atmospheric phenomena. Following chapter describes some methods to mitigate negative atmospheric phenomena affecting the FSO link. The second part of the thesis deals with the design of the support system for FSO, based on softcore microcontroller MicroBlaze, design of a simple network switch and a network interface for MicroBlaze. Lastly, software implementation of a web server and design of a web interface, allowing remote administration of the link and its components, are discussed.

KEYWORDS

Free space optical communication, atmospheric phenomena, LwIP, MicroBlaze

ABSTRAKT

Tato práce se zabývá problematikou optických bezkabelových spojů (FSO). V úvodní kapitole jsou diskutovány přednosti, základní principy a dílčí komponenty FSO spojů. Druhá kapitola se zabývá atmosférou z pohledu šířícího se optického svazku, jejím složením, základními veličinami a jevy v ní nastávajícími. V následující kapitole je popsáno několik metod ke zmírnění jevů majících negativní vliv na kvalitu spoje. Druhá část práce se zabývá návrhem podpůrného systému pro FSO, založeném na softcore mikroprocesoru MicroBlaze, návrhem jednoduchého síťového přepínače a síťového rozhraní. Závěr práce pojednává o implementaci webového serveru a tvorbě webové prezentace umožňující vzdálenou správu FSO a jeho komponent.

KLÍČOVÁ SLOVA

Bez kabelová optická komunikace, atmosférické jevy, LwIP, MicroBlaze

JANÍK, L. *Support system for administration and control of FSO transceiver*. Brno: Vysoké učení technické v Brně, Fakulta elektrotechniky a komunikačních technologií, 2016. 90 s. Vedoucí diplomové práce prof. Ing. Otakar Wilfert, CSc..

DECLARATION

I declare that I have written my master's thesis on the theme of "Support system for administration and control of FSO transceiver" independently, under the guidance of the master's thesis supervisor and using the technical literature and other sources of information which are all quoted in the thesis and detailed in the list of literature at the end of the thesis. As the author of the master's thesis I furthermore declare that, as regards the creation of this master's thesis, I have not infringed any copyright. In particular, I have not unlawfully encroached on anyone's personal and/or ownership rights and I am fully aware of the consequences in the case of breaking Regulation S 11 and the following of the Copyright Act No 121/2000 Sb., and of the rights related to intellectual property right and changes in some Acts (Intellectual Property Act) and formulated in later regulations, inclusive of the possible consequences resulting from the provisions of Criminal Act No 40/2009 Sb., Section 2, Head VI, Part 4.

Brno

.....
author's signature

ACKNOWLEDGEMENT

I would like to thank to my diploma thesis supervisor, prof. Ing. Otakar Wilfert, CSc. for his support, motivation and insightful comments. I would also like to thank to Ing. Michal Kubíček, Ph.D. for valuable suggestions and consultations about FPGAs. Special thanks goes to Bc. Marek Novák for many valuable discussions on the topic and the first review of the thesis. Finally, I must express my very profound gratitude to my family for providing me with unfailing support throughout my years of study and the process of writing this thesis.

Brno

.....
author's signature



Faculty of Electrical Engineering
and Communication
Brno University of Technology
Purkynova 118, CZ-61200 Brno
Czech Republic
<http://www.six.feec.vutbr.cz>

ACKNOWLEDGEMENT

Research described in this master's thesis has been implemented in the laboratories supported by the SIX project; reg. no. CZ.1.05/2.1.00/03.0072, operational program Výzkum a vývoj pro inovace.

Brno

.....

author's signature



EVROPSKÁ UNIE
EVROPSKÝ FOND PRO REGIONÁLNÍ ROZVOJ
INVESTICE DO VAŠÍ BUDOUCNOSTI



Contents

Preface	1
1 Free space optical communication	2
1.1 Motivation	2
1.2 Common measures	3
1.2.1 Signal to noise ratio	3
1.2.2 Bit error rate	3
1.2.3 Channel capacity	3
1.3 FSO performance	4
1.4 FSO transmitter	4
1.4.1 Laser	5
1.4.2 Gaussian beam	6
1.4.3 Transmitting optical system	7
1.5 FSO receiver	8
1.5.1 Photodetector	8
1.5.2 Receiving optics	10
1.6 FSO power balance	10
1.7 Summary	12
2 Atmosphere	13
2.1 Atmospheric composition	13
2.1.1 Gas components	13
2.1.2 Aerosols	14
2.2 Atmospheric conditions	15
2.2.1 Transmittance	15
2.2.2 Visibility	15
2.3 Atmospheric phenomena	16
2.3.1 Scattering	16
2.3.2 Scintillations	19
2.3.3 Molecular absorption	20
2.3.4 Aerosol absorption	22

2.3.5	Precipitation attenuation	25
2.4	Other phenomena	27
2.5	Summary	27
3	Methods for mitigation of atmospheric influences	28
3.1	Aperture averaging	28
3.2	Spatial diversity	29
3.2.1	Basic principle	29
3.2.2	Combining methods	30
3.2.3	Results	32
3.3	Adaptive optics	32
3.4	Channel coding and interleaving	33
3.4.1	Block codes	34
3.4.2	Convolutional codes	34
3.4.3	Interleaving	35
3.5	HVAC Unit	36
3.6	Summary	36
4	Support system for FSO	38
4.1	Preface	38
4.2	Initial design	38
4.2.1	XUPV5-LX110T Evaluation Platform (ML505)	39
4.2.2	Media Converter	40
4.3	Proposed solution	40
4.4	Frame switching	41
4.4.1	TEMAC Client interface	41
4.4.2	Flow Controller	43
4.5	MicroBlaze design	46
4.5.1	Design flow	46
4.5.2	Base design	50
4.5.3	Network interface	50
4.5.4	Optical path statistics	52
4.6	Software implementation	53
4.6.1	Software project hierarchy	54
4.6.2	LwIP	54
4.6.3	HTTP server	56
4.7	Climate control unit	59
4.7.1	Provided functionality	59
4.7.2	RS-485 Driver	60

4.7.3	Serial interface	60
4.7.4	Proposed improvements	61
4.8	Summary	62
Conclusion		63
Bibliography		64
List of symbols, physical constants and abbreviations		68
List of appendices		70
A	MicroBlaze project	71
B	Web UI	73
C	HVAC	75
C.1	Driver board	75
C.2	HVAC Unit commands	77
C.3	HVAC Improvements	77

List of Tables

1.1	Values of geometrical path losses for various distances [4]	8
1.2	Power balance contributions	11
2.1	Atmospheric layers	13
2.2	Radius and concentration ranges of common particles [10]	14
2.3	Q parameter values by Kruse model	17
2.4	Q parameter values by Kim model	18
2.5	Turbulence attenuation for 1km and 30km distances	20
2.6	Global transmission windows [4]	21
4.1	Software controllable temperature and humidity limits	59
A.1	Used IP cores (generic)	71
A.2	Used IP cores (custom)	71
C.1	RS-485 Driver board partlist	76
C.2	HVAC command list	77

List of Figures

0.0.1 Claude Chappe's optical telegraph [1]	1
1.3.1 Simplified model of FSO link	4
1.4.1 Stimulated emission [3]	5
1.4.2 Gaussian beam propagating along the Z axis	6
1.5.1 PIN diode structure [7]	9
1.5.2 The responsivity of common materials [8]	10
1.6.1 An example of a power balance diagram	12
2.3.1 Comparison of ROF and calculated fog attenuations[13]	18
2.3.2 Influence of variable sized inhomogenities	19
2.3.3 Transmittance of the atmosphere due to molecular absorption[15]	21
2.3.4 Common cloud types[16]	23
2.3.5 Specific attenuation of different cloud types [17]	23
2.3.6 Cummulative distribution function for two months[18]	24
2.3.7 Comparison of M-P and Carbonneau distributions[19]	26
2.3.8 Specific attenuation of a snow at different wavelengths[20]	26
3.1.1 BER vs. aperture diameter under various weather conditions [22]	29
3.2.1 Received intensity as a function of time[23]	30
3.2.2 Comparison of combining methods [24]	31
3.2.3 BER vs the number of receivers [22]	32
3.3.1 Two common approaches of AO[25]	33
3.3.2 Effect of AO on focal plane power distribution [26]	33
3.4.1 An example of convolutional coder [27]	35
3.4.2 Deinterleaving principle	36
4.1.1 Simplified system scheme	38
4.2.1 XUPV5-LX110T Evaluation Platform [29]	39
4.2.2 Main data line block scheme with interfaces	40
4.4.1 TEMAC Client interface - Client transmission sequence	42
4.4.2 TEMAC Client interface - Client reception sequence	43
4.4.3 Flow Controller read-out (R) and write-in (W) state machines and data FIFOs. Modified or added parts are highlighted in red.	44
4.4.4 Frame for MicroBlaze being processed in Flow controller	44

4.5.1 XPS - Used MicroBlaze IP cores in Bus interfaces panel	47
4.5.2 XPS - IP core IO ports	47
4.5.3 XPS - MicroBlaze address space and IP core address mapping	50
4.5.4 Block RAM signals [30]	51
4.5.5 Control data line - connection of MicroBlaze to Flow Controller FIFOs. XPS BC - XPS BRAM Controller IP core. CTRL - Custom IP core for control of the communication between the MicroBlaze and the BRAM controller	52
4.5.6 Link State Frame format	53
4.6.1 An example of ARP and ICMP communication between PC (192.168.1.13) and LwIP at MicroBlaze (192.168.1.16)	56
4.6.2 The first version of simple web interface with top level counters. Only SSI used.	57
4.6.3 Current version of web interface	58
4.7.1 Schema of the RS-485 driver board	60
4.7.2 Positioning of the RS-485 driver on pinheaders J5 and J6	60
B.0.1 Web UI - Statistics	73
B.0.2 Web UI - Configuration	73
B.0.3 Web UI - HVAC configuration	74
B.0.4 Web UI - About	74
C.1.1 RS-485 Driver board - Assembly, scale 2:1	75
C.1.2 RS-485 Driver board - Layout, scale 1:1	75
C.1.3 Assembled RS-485 Driver board	76
C.3.1 Theoretical construction of HVAC with Peltier element	77

PREFACE

An optical communication presents a perspective, non-pollutive and licence-free communication technique. Since an invention of the laser and the dramatical reduction of optical fibre losses, optical connections play the main role in the field of the fastest connectivity and replaced most of metallic backbone connections.

Origins of optical communications stretch hundreds of years back, starting with primitive binary signals represented by smoke or fire signals on hilltops. Compared to preceding days, when the only possible message delivery method was sending a messenger on a horseback, this method provided an advantage in its low propagation time. The elementary information was transferred to distances of tens of kilometers as fast, as the remote observer could notice it, however amount of the transferred information per time unit was very low. The great turn came many years later - at the end of 18th century, with the invention of Claude Chappe's optical telegraph. Yet the basic principle remained the same, the amount of transferred information was significantly increased by the use of greater symbol alphabet. Chappe's telegraph consisted of three adjustable wooden arms, built atop of stone tower. These arms could take various angles; from these positions Chappe assembled telegraph symbol alphabet consisting of 92 symbols. This invention is nowadays considered to be the beginning of telecommunications, the trend of increasing symbol count or symbol transfer speed remains.

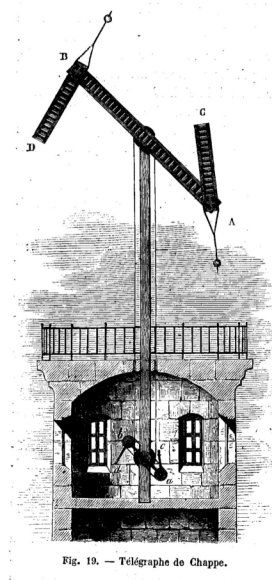


Fig. 0.0.1: Claude Chappe's optical telegraph [1]

1 FREE SPACE OPTICAL COMMUNICATION

A free space optical link represents an optical wireless connection, mostly with the Earth's atmosphere as the main propagation environment. The information is modulated on single or multiple optical carriers located on single or multiple optical beams. These links could be employed in various situations - they allow point to point or point to multi-point communication, ground to satellite, satellite to satellite and underwater communication, they can be either mobile or stationary. Further in this thesis, terrestrial point to point, full-duplex, stationary link will be discussed.

1.1 Motivation

The free space optical communication provides a considerable solution for last-mile links where wireless technologies are commonly used, due to lower costs in comparison to wired technologies where excavation works are needed to be done. Wireless connections also bring the possibility to connect places where wired connections are impossible due to terrain conditions. Wireless connections can be put into service very fast and mounting them to existing antenna masts is also possible, leading to further discounts. According to this fact, RF and microwave links are massively used.

Modern digital modulations approaches the communication speed of microwave connections to the theoretical Shannon limit, causing demand on the increase of carrier frequency and bandwidth. While the theoretical communication channel transfer rate is proportional to the carrier bandwidth and frequency, the transfer from RF or microwave band to the light spectra brings theoretical increase of the transfer rate up to five orders higher [2]. The increase of the carrier frequency also affects the required aperture (antenna) size and directivity which are directly proportional to the used wavelength.

Compared to wireless RF connections, an optical links bring plenty of advantages, namely:

- Non-licensed operation
- Higher transfer rates
- Higher energy and spectral efficiency
- Smaller transceivers
- Durable to sniffing or exploiting

- No electromagnetic interference
- Operation with reciprocal channel

Similarly to RF connections, the quality of a FSO connection is significantly dependent on channel conditions, but effects of particular phenomena on FSO and RF or microwave channels differ. This fact is employed in hybrid systems, which consist of a FSO transceiver, establishing the main communication channel and a RF transceiver as a limited rate assistance link in cases of bad weather conditions.

1.2 Common measures

1.2.1 Signal to noise ratio

The Signal to Noise Ratio (SNR) is a common measure for estimating the channel quality. The SNR compares the level of an observed signal relatively to a noise level. The SNR is in logarithmic nature defined as:

$$SNR = 10 \cdot \log \frac{P_{sig}}{P_{noise}} \quad [dB] \quad (1.1)$$

1.2.2 Bit error rate

The Bit Error Rate (BER) in digital communications is a common measure for estimating the transaction quality. The bit error rate is defined as a fraction of erroneously transferred bits to the number of all transmitted bits, during previously defined measuring time.

$$BER = \frac{N_{err}}{N_{tot}} \quad [-]$$

The BER is proportional to the SNR.

1.2.3 Channel capacity

A channel capacity, defined by Shannon-Hartley theorem is defined as the theoretical upper bound of the data rate of a communication channel with the bandwidth B and noise conditions defined by the SNR:

$$C = B \log_2 (1 + SNR) \quad [b/s] \quad (1.2)$$

1.3 FSO performance

To ensure high data rates, a well-calculated power balance as well as an adequate electronic front-end are required. As you can see in fig. 1.3.1, input electrical signal is brought to the transmitter and transferred to the optical spectra by modulation on an optical beam with mean radiated optical power $P_{m,TX}$. The beam is propagating against the receiver, total losses along the path are summarized in α_{tot} , total gains along the path are summarized in γ_{tot} . A beam with the received mean optical power $P_{m,RX}$ illuminates the photodetector, which transfers it back to an electrical signal.

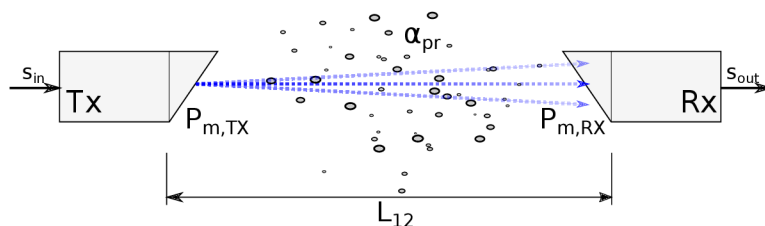


Fig. 1.3.1: Simplified model of FSO link

A simplified power balance can be in logarithmic sense expressed as:

$$P_{m,RX} = P_{m,TX} - \alpha_{tot} + \gamma_{tot} \quad (1.3)$$

In a real situation, all of these power contributions (positive and negative) are much more complex and consist of many components.

It is obvious, that to reach the required amount of the received optical power, the transmitting power must be increased while propagation losses must be decreased. Whereas the transmitted power is dependent on the used light source, propagation losses are proportional to the square of distance and are considerably affected by conditions and composition of the propagation environment. These conditions will be discussed later in chapter 2, which deals with an atmosphere as the essential propagation environment of terrestrial FSO links.

1.4 FSO transmitter

Thanks to its power, spectral and spatial properties, lasers are almost exclusively used as an optical transmitter for free space optical links.

1.4.1 Laser

Lasers are quantum devices whose function is based on a stimulated emission (see fig. 1.4.1).

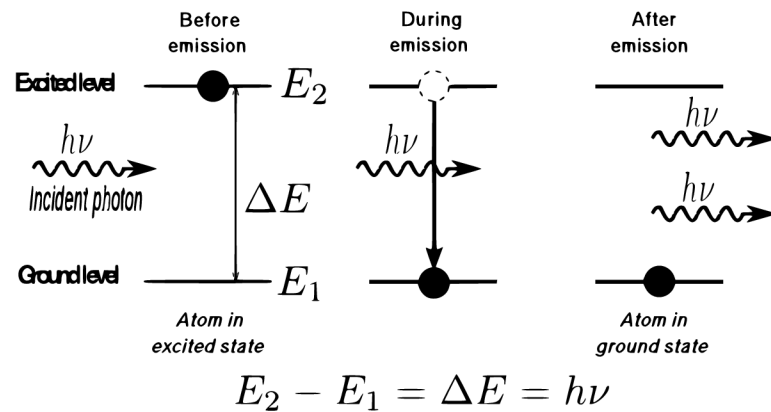


Fig. 1.4.1: Stimulated emission [3]

Three essential laser components are: a power source, a resonator and an active medium. Electrons (carriers), present on the lower energy level, are receiving the energy from the source which pushes them to a higher energy layer (absorption). A single carrier, decaying to lower energy level (recombination), is accompanied by a photon emission. The average time, which takes the carrier to spontaneously recombine, is called a lifetime τ . A carrier, recombining without an external affection, causes a so called *spontaneous emission* (undesirable), which is participating on output intensity fluctuations. The emitted photon, moving near the carrier at the excited energy level, can also initiate the recombination (wanted), causing emission of an another photon. This emission is called *stimulated emission* and causes the coherence matter of a laser beam. Emitted photons are traveling between resonator mirrors, tearing down more excited electrons. The reflectance of one of mirrors is intentionally decreased, which allows a small part of photons to leave the resonator at the cost of slight decrease of the resonator gain.

Laser types

Common laser types, distinguished by active medium are:

- solid lasers (YAG-Nd)
- gas lasers (He-Ne)
- semiconductor lasers

The light intensity of solid and gas lasers cannot be directly affected (only by external modulators), whereas semiconductor lasers have a great advantage, because their

radiant power and optical frequencies can be directly modulated by the injection current [4]. Semiconductor lasers are also more size- and cost- effective. However, whereas internal modulation methods can reach modulation speeds of few Gb/s, external modulators could operate at tens of Gb/s and can also provide more sophisticated modulation methods [5].

Operating wavelength

The wavelength of a Laser beam is one of the essential things to consider when designing an optical link, especially due to molecular absorption of the atmosphere (see chapter 2). The transmission of an atmosphere is dependent on the wavelength of the propagating beam; there are several wavelength ranges, where atmospheric attenuation reaches acceptable values (less than 0.2 dB/km), these ranges are called *atmospheric transmission windows*. The majority of FSO systems is designed to operate in transmission windows of $780 \text{ nm} - 850 \text{ nm}$ and $1520 \text{ nm} - 1600 \text{ nm}$ [2].

1.4.2 Gaussian beam

In order to fully understand the problematics of a beam propagation, the optical beam used to carry the information should be defined first.

A laser beam leaving a laser diode can be successfully approximated by a gaussian beam. The optical power of a gaussian beam, propagating along z axis, is concentrated into a narrow cone and its transverse optical intensity is defined by a circularly symmetric gaussian function, with I_0 as the maximum on the propagation axis [6].

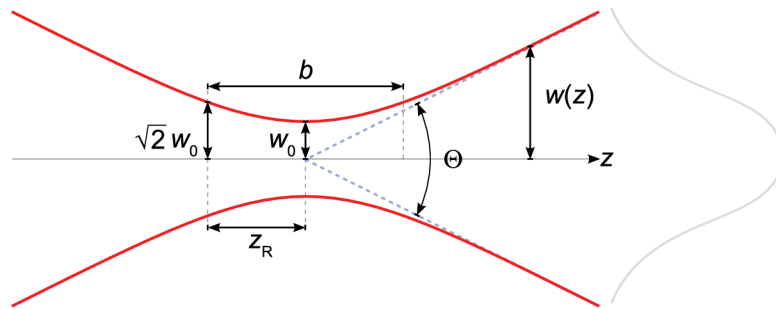


Fig. 1.4.2: Gaussian beam propagating along the Z axis

A beam half-width is defined as:

$$w(z) = w_0 \sqrt{1 + \left(\frac{z}{z_R}\right)^2} \quad [m] \quad (1.4)$$

The function $w = f(z)$ is illustrated in fig. 1.4.2, here w_0 stands for a beam waist which is half-width of the beam at its focus ($z = 0$), A Rayleigh distance z_R is the distance, where the half-width is equal to:

$$w = \sqrt{2} \cdot w_0 \quad [m] \quad (1.5)$$

An angle formed by single diverging edge of the cone and the propagation axis is called an angle of divergence and is defined as:

$$\theta = \lim_{z \rightarrow \infty} \frac{w(z)}{z} = \frac{\lambda}{\pi w_0} \quad [rad] \quad (1.6)$$

For distances $z \gg z_R$, $w = f(z)$ becomes linear and the beam can be taken as a spherical wave originated from the beam focus.

A total angular spread of a beam is then defined as:

$$\Theta = 2\theta \quad [rad] \quad (1.7)$$

If the non-linear influence of a propagation medium is neglected, the gaussian nature of the beam remains preserved and only the optical intensity and the beam width changes along the direction of propagation. An optical intensity along the propagation axis is equal to:

$$I(0, 0, z) = \frac{I_0}{1 + \left(\frac{z}{z_R}\right)^2} \quad [W/m^2] \quad (1.8)$$

Which can be for distances $z \gg z_R$ simplified to:

$$I(0, 0, z) \approx I_0 \cdot z_R^2 \cdot \frac{1}{z^2} \quad [W/m^2] \quad (1.9)$$

As you can see in eq. 1.9, the intensity is decreasing with square of the distance, which causes great beam attenuation, contributing to propagation losses.

1.4.3 Transmitting optical system

The divergence of a laser beam causes the receiver to collect only a part of the emitted energy, this attenuation is called *geometric path loss* α_{geom} . A geometric path loss together with atmospheric losses forms a *propagation loss* α_{pr} . A geometric path loss is defined as [4]:

$$\alpha_{geom} = 10 \cdot \log \frac{S_b}{S_r} = 10 \cdot \log \frac{\frac{\pi}{4} \cdot (d\Theta)^2}{S_r} \quad [dB] \quad (1.10)$$

Here Θ is a divergence of the beam, d is distance between the transmitter and the receiver, S_r is an area of the receiver aperture and S_b is an area of the beam at distance d .

Tab. 1.1: Values of geometrical path losses for various distances [4]

Divergence	Distance	α_{geom}
1 <i>mrad</i>	5 <i>km</i>	29 <i>dB</i>
3 <i>mrad</i>	2 <i>km</i>	37 <i>dB</i>
1 <i>mrad</i>	8 <i>km</i>	33 <i>dB</i>

To decrease the divergent matter of a laser beam, convergent lenses are used. Efficiency of the coupling between a laser diode and an optical system depends on the beam distribution and the divergence and can be evaluated as:

$$\alpha_{coup,tx} = \left| 10 \cdot \log \frac{P_{tos}}{P_{LD}} \right| \quad [dB] \quad (1.11)$$

Where P_{tos} is the optical power incident on a transmitting optical system and P_{LD} is the optical power leaving a laser diode. Practically, this efficiency equals to 1.5 *dB* [4].

1.5 FSO receiver

1.5.1 Photodetector

Photodetectors are mostly semiconductors, responsible for detecting a modulated beam by acting as a light-sensitive resistances or voltage or current sources. There are many types of photodetectors, based either on direct or indirect (e.g. coherent homodyne receiver) detection. Direct-detection PIN diodes are most commonly used for high speed optical communications [5].

A PIN diode consists of a semiconductive P-N junction with an intrinsic (undoped) region between P and N areas. As a photodetector, the PIN diode is biased reverse, not participating on the conduction. An incident light (photon flux) enters the detector volume; each photon with a sufficient energy causes an absorption, releasing

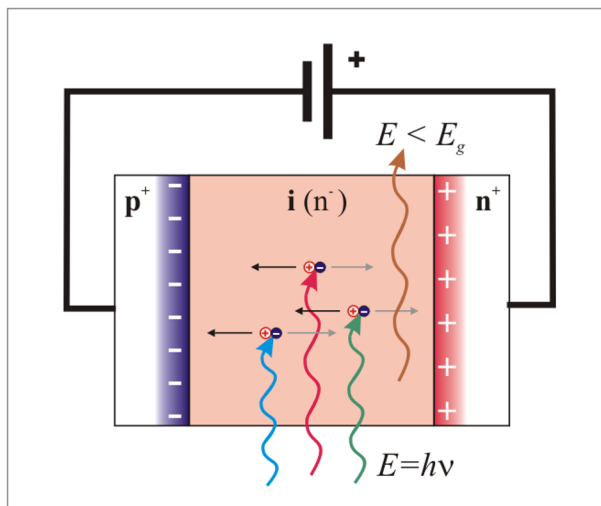


Fig. 1.5.1: PIN diode structure [7]

a pair of carriers. If an external electric field is present, those free carriers are separated and consequently participate on current conduction (photocurrent) [4]. If the diode does not operate at saturation, the photocurrent is directly proportional to the amount of incident light, however even if no incident light is present on the active surface of the diode, a small amount of current, called *dark current* is passing through the diode. This current increases with junction temperature and together with shot noise and thermal noise participates on decreasing the system SNR.

A mean photocurrent \bar{i} , caused by an incident light, is proportional to an incident optical power P_{PD} and a photodetector responsivity R_i :

$$\bar{i} = R_i \cdot P_{PD} \quad [A] \quad (1.12)$$

The responsivity of the photodetector is dependent on the wavelength and the quantum efficiency of the detector η :

$$R_i = \frac{e \cdot \eta}{\hbar \cdot \omega} \quad [A \cdot W^{-1}] \quad (1.13)$$

Where η is defined as:

$$\eta = \frac{\text{number of generated electron-hole pairs}}{\text{number of incident photons}} \quad [-] \quad (1.14)$$

The responsivity is dependent upon the material, this material should be chosen with a bandgap energy slightly less than the energy of an incident optical wavelength. This leads to satisfiable compromise between a responsivity and a dark current.

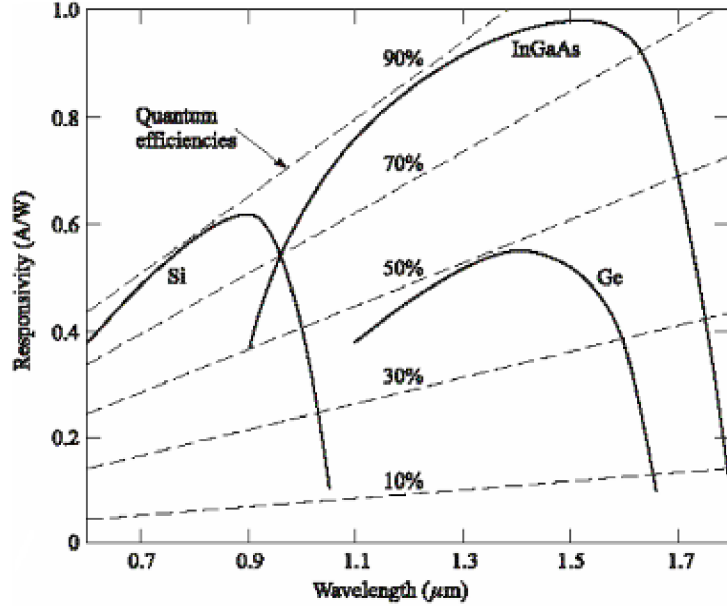


Fig. 1.5.2: The responsivity of common materials [8]

1.5.2 Receiving optics

A receiving optical system focuses incident optical beam onto active surface of the photodetector and thus increases the amount of the incident optical power. This contribution is called a receiving optical system gain and equals to [9]:

$$\gamma_{ros} = \left| 20 \cdot \log \frac{D_{ROS}}{D_{TOS}} \right| + 3 \quad [dB] \quad (1.15)$$

In the equation, the $+3dB$ gain is caused by different shape of the wavefront at the receiver and the transmitter. Whereas at the transmitter the beam has a gaussian energy distribution with distinct maximum near the propagation axis, the incident wave at the receiver can be taken as a plane wave. The quality of the coupling between the optics and the photodetector is described by a receiving optical system coupling. This coupling is dependent on the fraction of the active surface of the photodiode and the incident laser spot size. This coupling is equal to zero when $A_{PD} \leq A_{spot}$.

1.6 FSO power balance

A FSO power balance is the first step in a FSO link design, where all particular power contributions are calculated and the power balance equation is assembled. Thanks to a power balance equation, one gains overview about power conditions at

particular parts of the link. A power balance diagram is a graphical representation of particular contributions and brings increased lucidity to the design. A power balance consists of:

Tab. 1.2: Power balance contributions

Symbol	Name
P_{LD}	Laser diode mean optical power
$\alpha_{coup,tx}$	Transmitting optical system coupling efficiency
α_{tos}	Transmittance of the transmitting optical system
α_{geom}	Geometric path loss
α_{atm}	Atmospheric losses
α_{ros}	Transmittance of the receiving optical system
γ_{ros}	Gain of the receiving optical system
$\alpha_{coup,rx}$	Receiving optical system coupling efficiency
ρ_{atm}	Reserve for atmospheric phenomena
P_0	Receiving system sensitivity

With contributions listed in table 1.2, the power balance equation can be assembled:

$$P_{m,RX} = P_{LD} - \alpha_{coup,tx} - \alpha_{tos} - \alpha_{geom} - \alpha_{atm} - \alpha_{ros} + \gamma_{ros} - \alpha_{coup,rx} - \rho_{atm} \quad [dBm] \quad (1.16)$$

In this equation, the received power level $P_{m,RX}$ is commonly substituted with a receiving system sensitivity P_0 , which is defined as minimal received power needed to reach defined SNR:

$$P_0 = P_{min} + SNR_0 \quad [dBm] \quad (1.17)$$

Where P_{min} stands for a minimal detectable power on the photodetector. A receiver saturation power P_{max} must be also considered since the received optical power must at all atmospheric conditions stay in the range from P_{min} to P_{max} (dynamic range Δ_P). Violation of this rule would lead to increase of BER even during good atmospheric conditions.

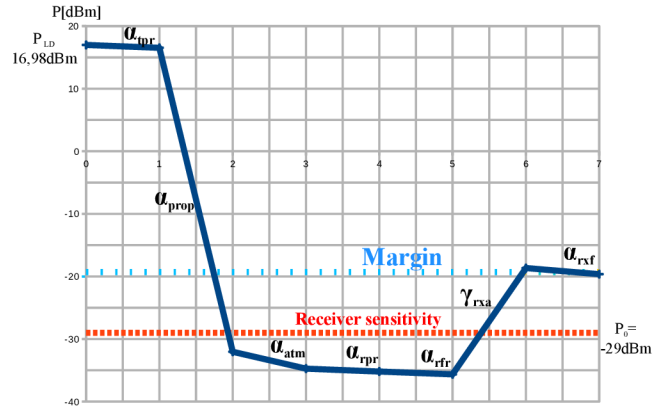


Fig. 1.6.1: An example of a power balance diagram

1.7 Summary

The first chapter makes a brief introduction into the problematics of a free space optical communication. Common measures and basic principles are introduced. The first chapter also discusses key components of a FSO transceiver with emphasis on their properties. As the result, a FSO power balance is introduced, containing contributions from all discussed FSO components. A power balance as well as context of entire chapter is of static nature, overall losses, gained from worst-case results of (mostly) statistical data are balanced by sufficient power margin, which is not efficient.

2 ATMOSPHERE

An atmosphere (from Greek word *atmos*, meaning vapour) is a set of concentric gas layers surrounding Earth¹. The atmosphere is retained by Earth's gravity and its density is thus dependent on the distance from the surface.

Common atmospheric layers are listed in table below. They differ in the composition, the temperature gradient and the density. We are most interested in the troposphere as the undermost layer with the biggest particle and gas density, where most of atmospheric phenomena occur [4].

Tab. 2.1: Atmospheric layers

Layer	Altitude
Troposphere	0 km to 12 km
Stratosphere	12 km to 50 km
Mesosphere	50 km to 80 km
Thermosphere	80 km to 700 km
Exosphere	700 km to 10 000 km

An atmosphere represents a heterogeneous anisotropic lossy medium, changing its properties in time, which significantly influences an incident optical beam.

2.1 Atmospheric composition

2.1.1 Gas components

The atmosphere consists of various atoms and molecules. Its gas components can generally be divided into two categories [4]:

- components with fixed density proportion or majority components, especially:
 - N_2 - 78%
 - O_2 - 21%
 - Ar - 0,9%
 - CO_2 - 0,03%
- components with variable density (the concentration depends on the geographical location), e.g. water vapor, O_3 - 0% - 4%

¹An atmosphere can also surround any sufficiently massive object

2.1.2 Aerosols

Aerosols are small solid or liquid particles suspended into an atmosphere. Their size varies from few nanometers to tens of micrometers; they drift from the stratosphere to the surface and their lifetime is variable, dependent on particles' weight (lighter particles are less attracted to the ground and have longer lifetime).

Aerosols can be divided according to their origin onto:

- natural aerosols
 - volcanic aerosols
 - dust
 - sea salts
 - various forms of condensed water
- human-made aerosols
 - smoke
 - sulfates

While sea salts and desert dust tend to be greater in size, they have shorter lifetime (few days) and their range is thus local. Volcanic aerosols, caused by major volcanic eruptions, can be dragged into stratosphere and remain there for up to 2 years (converted to droplets of sulfuric acid).

Tab. 2.2: Radius and concentration ranges of common particles [10]

Type	Radius [μm]	Concentration [cm^{-3}]
Air molecules	10^{-4}	10^{19}
Solid particles	10^{-2} to 1	10 to 10^3
Fog	1 to 10	10 to 100
Cloud	1 to 10	100 to 300
Raindrops	10^2 to 10^4	10^{-5} to 10^{-2}
Snow	10^3 to $5 \cdot 10^3$	–
Hailstones	$5 \cdot 10^3$ to $5 \cdot 10^4$	–

A **Fog** is a cloud of very small particles of water, suspended into air, floating near ground. A fog reduces visibility to less than 1km. A fog forms when the difference between the air temperature and the dew point is generally less than 2.5 °C [11].

A **Mist** are small droplets of a condensed water, suspended into air. The condensation is caused by sudden cooling of warm, humid air (winter exhaling).

A **Haze** is caused by suspending combination of dry aerosols (smoke,dust,ash) into air, wich leads to mitigation of the visibility.

2.2 Atmospheric conditions

2.2.1 Transmittance

A transmittance τ is the ability of propagation environment to pass a light through it and is defined as a fraction of the emitted light power $P(0)$ and the power leaving examined medium $P(d)$, at distance d from the transmitter:

$$\tau(d) = \frac{P(d)}{P(0)} = e^{-\sigma d} \quad [-] \quad (2.1)$$

2.2.2 Visibility

A visibility was defined for meteorological needs as an estimated distance, at which an observer can just see some reference marker. For optical purposes, the visibility is deposing about the atmosphere transparency, which is closely related to weather conditions. This method is subjective, dependent on many factors and with no strict rules. To eliminate the subjective matter of preceding observations, a *meteorological optical range* or a visibility V with strictly defined measuring methods was established, providing objective, repeatable measurements.

In the atmosphere, a meteorological optical range is the distance, that a parallel luminous ray beam, emanating from an incandescent lamp, at a color temperature of 2700K, must reach so that the luminous flux intensity is reduced to 0.05 if its original value [4].

A MOR can be measured by transmissometers, whose principle is based on emitting a known optical power and measuring an amount of light incident at photodetector. Transmissometers are constructed either with transmitter-receiver or transceiver-mirror topologies.

A visibility is closely related to a transmittance; this relation is further discussed later in section dealing with Mie scattering.

2.3 Atmospheric phenomena

Essential phenomena influencing an optical beam are:

- Scintillations - a heated air rising from the ground causes variability of air refractive index (turbulence), leading to beam magnitude fluctuations
- Scattering - interaction of a light and particles causing directional beam redistribution
 - Rayleigh scattering - particles are equal or smaller size than the beam wavelength
 - Mie scattering - particles are of the same order of magnitude as the beam wavelength
- Absorption - a part of incident light is transformed to a heat or a chemical energy, decreasing the beam magnitude.

The influence of scattering and absorption is summarized by *extinction coefficient* σ defined as:

$$\sigma = \alpha_m + \alpha_n + \beta_m + \beta_n \quad [km^{-1}] \quad (2.2)$$

Where α_m stands for a molecular absorption coefficient representing the molecular absorption, α_n is an absorption of aerosols and β_m, β_n are Rayleigh and Mie scattering coefficients.

2.3.1 Scattering

A scattering of a light deflects the ray from its previous path by interaction with particles or on different refractive index borders. Rayleigh, Mie, Tyndall, Brillouin and Raman scattering are distinguished, however only Rayleigh and Mie are important to a FSO.

Rayleigh scattering occurs when an optical beam interacts with particles of equal or smaller size than the beam wavelength. One of examples of Rayleigh scattering is the interaction between the sunlight and molecules of atmosphere gases. While a solar beam with a broad spectrum is making a way through the atmosphere, some wavelengths, defined by the atmospheric composition, are scattered. Since shorter wavelengths visible as blue color are more scattered, the clear sky is colored with blue. A similar effect causes the sunrise and the sunset being colored red. At this

case the solar beam is traveling significantly longer distance, causing most of the shortest wavelengths being scattered out, leaving only the longer wavelengths.

Rayleigh scattering negatively affects a laser beam, increasing total atmospheric attenuation. Thanks to the knowledge of the atmospheric composition, a molecular scattering coefficient β_m can be approximately obtained [4]:

$$\beta_m(\alpha) = A \cdot \lambda^{-4} \quad [km^{-1}] \quad (2.3)$$

$$A = 1,09 \cdot 10^{-3} \frac{P}{P_0} \frac{T_0}{T} \quad [km^{-1} \mu m^{-1}] \quad (2.4)$$

Where $P[mbar]$ is an atmospheric pressure, $P_0 = 1013.25 \text{ mbar}$ is the atmospheric pressure at sea level, $T[K]$ is an atmospheric temperature and $T_0 = 273.15K$ is a reference temperature. At 1600 nm , $20 \text{ }^\circ\text{C}$ and the sealevel pressure, this gives the result of $1.744 \cdot 10^{-5} km^{-1}$. This leads to conclusion that the attenuation caused by Rayleigh (molecular) scattering at infrared spectrum, where all common lasers operate, is negligible.

Mie scattering occurs when an optical beam interacts with particles whose size is comparable to the beam wavelength. The major contributors to Mie scattering in atmosphere are aerosols, especially particles of condensed water (mist,fog). The essential problem in evaluating a scattering coefficient is that concentration and size of aerosols varies in time and space.

The solution is the use of visibility as the rule of proportion to aerosols concentration. The Mie (aerosol) scattering coefficient β_n can then be expressed as [4][12]:

$$\beta_n = \frac{3.91}{V} \left(\frac{\lambda_{nm}}{550_{nm}} \right)^{-Q} \quad [km^{-1}] \quad (2.5)$$

where V stands for a visibility, λ_{nm} is a wavelength in nanometers and Q is a scattering particle size distribution parameter. The Q parameter can be modeled either by Kim or Kruse model.

Tab. 2.3: Q parameter values by Kruse model

Q parameter	visibility range
1.6	$> 50 \text{ km}$
1.3	$6 \text{ km to } 50 \text{ km}$
$0.585V^{1/3}$	$0 \text{ to } 6 \text{ km}$

Since the Q values from table 2.3 were defined from haze particles (and thus from long visibilities), this model is considered not to be accurate enough for foggy situations.

Tab. 2.4: Q parameter values by Kim model

Q parameter	visibility range
1.6	> 50 km
1.3	6 km to 50 km
$0.16V + 0.34$	1 km to 6 km
$V - 0.5$	0.5 km to 1 km
0	< 0.5 km

The table 2.4 contains modified values suitable also for lower visibilities.

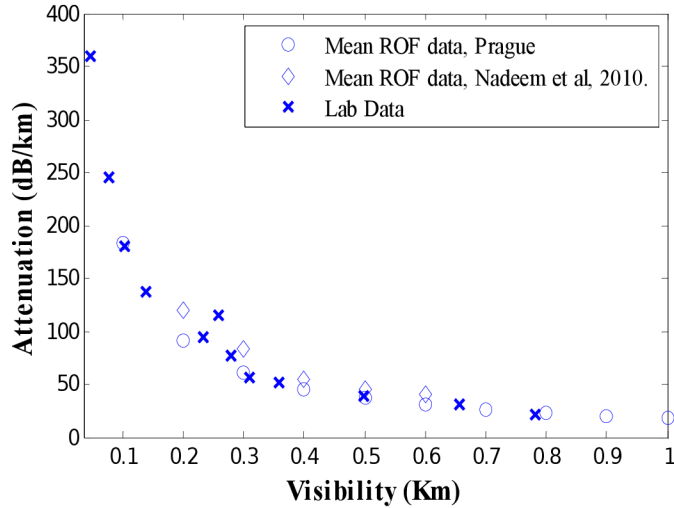


Fig. 2.3.1: Comparison of ROF and calculated fog attenuations[13]

With the knowledge of previous facts, it is obvious that Mie scattering could cause an enormous attenuation to a laser beam and presents crucial part of the extinction coefficient. With sufficiently low values of the molecular and the aerosol absorption and Rayleigh scattering, those can be neglected and the extinction coefficient can be considered as equal to the Mie scattering coefficient:

$$\sigma \cong \beta_n \quad (2.6)$$

An attenuation in logarithmic domain can be calculated by:

$$\alpha_{ext,dB} = 0.23\sigma \quad [dB] \quad (2.7)$$

2.3.2 Scintillations

A scintillation is a flash of light, produced in a transparent material by the passage of a particle [10].

A **turbulence** is an invisible air mass movement caused by collision of two parts of air with different direction and/or velocity. This phenomenon is generally caused by hot air rising above the hot surface (deserts, roads, parkings). Turbulences differ in temperature and size, which varies from few centimeters to hundreds of meters.

Turbulences are causing local changes to an air refractive index by local temperature and atmospheric pressure fluctuations, leading to random beam scattering and multipath propagation. If those inhomogeneities are larger than the incident beam, the beam is deviated (beam wander). In opposite case, the beam is widened (scattered). In practice, various sizes of inhomogeneities are present at the same time and both previously mentioned effects thus apply.

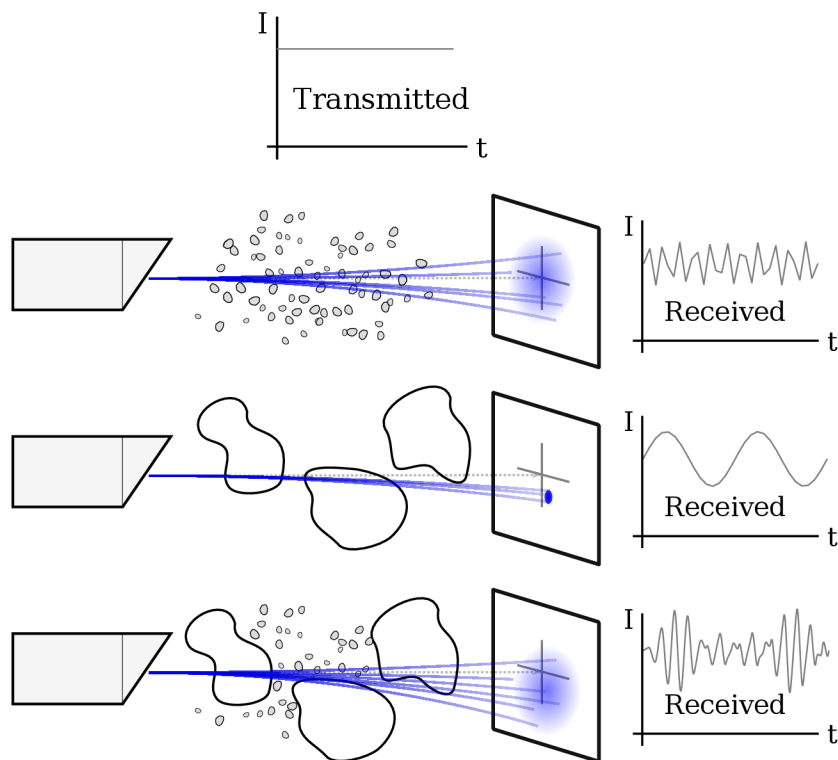


Fig. 2.3.2: Influence of variable sized inhomogeneities

Turbulences are mostly analyzed by statistical methods. By the use of Kolmogorov model, turbulent phenomena are described by a Kolmogorov structural function D_n , which is defined as:

$$D_n = C_n^2 r^{\frac{2}{3}} \quad \text{for } l_0 \ll r \ll L_0 \quad [-] \quad (2.8)$$

C_n^2 stays for a *structural parameter of the refractive index*, which describes turbulence intensity and is estimated from on meteorological data. An atmosphere without turbulences has $C_n^2 = 0$. r is the distance between the transmitter and the receiver and l_0 and L_0 is the minimal and maximal size of the turbulence.

Consequently, a relative scintillation fluctuation can be expressed as [14]:

$$\sigma_{I,rel}^2 = K \cdot C_n^2 \cdot k^{\frac{7}{6}} \cdot L_{12}^{\frac{11}{6}} \quad (2.9)$$

K is constant of the wave (1.23 for a plane wave, 0.5 for a spherical wave), k is a wave number and L_{12} is the distance between the transmitter and the receiver.

For a plane wave, a low turbulence and a specific receiver, the attenuation caused by turbulences can be evaluated as [14]:

$$\alpha_{turb} = 2 \cdot \sqrt{23.17 \left(\frac{2\pi}{\lambda}\right)^{\frac{7}{6}} C_n^2 L_{12}^{\frac{11}{6}}} \quad [db/km] \quad (2.10)$$

Common attenuation values per 1km for appropriate wavelengths and structural parameters are shown in the table 2.5

Tab. 2.5: Turbulence attenuation for 1km and 30km distances

Turbulence	Low	Moderated	High
$C_n^2 [m^{-2/3}]$	10^{-16}	10^{-14}	10^{-13}
$\alpha_{turb}(\lambda = 980 \text{ nm}) [dB/km]$	0.51	5.06	16.00
$\alpha_{turb}(\lambda = 1550 \text{ nm}) [dB/km]$	0.39	3.87	12.25

Further models are discussed in [14].

2.3.3 Molecular absorption

A molecular absorption is caused by the interaction between an incident light and molecules of the atmosphere. The absorption coefficient depends on character and density of molecules. Selective character of this absorption is obvious in fig. 2.3.3.

Molecules of atmospheric gases have discrete energy levels, whose distribution (energy) is dependent on its compound. An incident photon with energy $E = h \cdot \nu$,

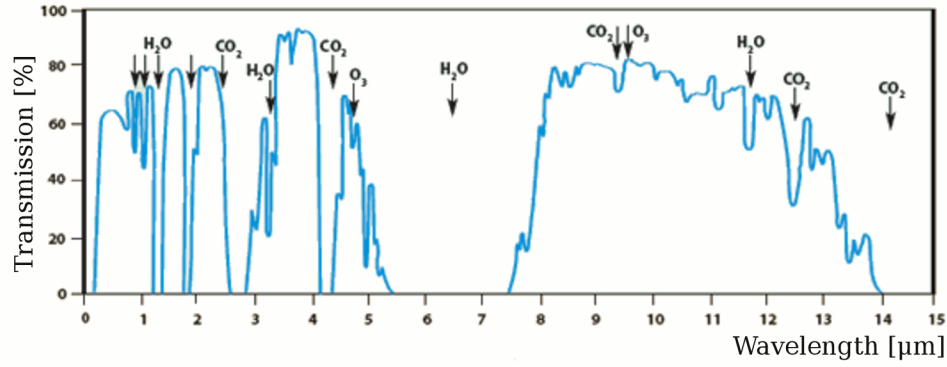


Fig. 2.3.3: Transmittance of the atmosphere due to molecular absorption[15]

corresponding to energy layers difference of the molecule, gets absorbed simultaneously, together with exciting electron at the lower layer. This phenomena is expressed as:

$$\nu = \frac{E_2 - E_1}{h} \quad [Hz] \quad (2.11)$$

Where ν stands for a photon frequency, h is Planck's constant and E_1 and E_2 are energy layers of the incident molecule. The width of spectral windows is affected by Doppler effect caused by the movement of molecules relatively to the radiation and pressure and temperature fluctuations.

There are few wavelength ranges where the absorption drops to values lower than $0.2dB$, these regions are called *transmission windows*. Global transmission windows corresponding with fig. 2.3.3 are mentioned in the table 2.6.

Tab. 2.6: Global transmission windows [4]

Band	Wavelength range [μm]
Visible to very near IR	0.4 – 1.4
Near IR or IR I.	1.4 – 1.9 and 1.9 – 2.7
Mean IR or IR II.	2.7 – 4.3 and 4.5 – 5.2
Far IR or IR III.	8 – 14
Extreme IR or IR IV.	16 – 28

2.3.4 Aerosol absorption

Aerosols increase an atmosphere attenuation by the scattering, which was discussed in Mie scattering theory above. An another part of the aerosol attenuation is caused by an aerosol absorption. The aerosol absorption is described by an aerosol absorption coefficient α_n which is dependent on an absorption cross section Q_a , unlike Mie scattering theory, where the scattering particle size distribution parameter Q was used.

The absorption cross section presents the probability of a molecule to absorb a photon of a particular wavelength and polarization. The absorption coefficient is given by following equation [4]:

$$\alpha_n(\lambda) = 10^5 \int_0^\infty Q_a \left(\frac{2\pi r}{\lambda}, n'' \right) \pi r^2 \frac{dN(r)}{dr} dr \quad [km^{-1}] \quad (2.12)$$

Here n'' is the imaginary part of the refractive index n of an aerosol, $r[cm]$ is the radius of particles and $dN(r)/dr[cm^{-4}]$ is the particle size distribution per unit of volume.

For optical beams in a visible and near infrared band, the imaginary part of refractive index is very low, contribution of the aerosol absorption to overall atmospheric attenuation and extinction coefficient thus can be neglected [4].

Cloud attenuation

A cloud is floating mass of condensed water (and chemicals) in form of droplets and frozen crystals. The concentration of those varies at $100 \text{ cm}^{-3} - 300 \text{ cm}^{-3}$ (vid. table 2.2). Common cloud types and their heights above sea level are shown in fig. 2.3.4.

The attenuation of clouds is basically caused by Mie scattering. According to Mie theory, discussed in scattering section, the cloud attenuation is calculated based on the knowledge of the scattering coefficient, calculated from the visibility and the size distribution parameter Q which are obtained from Kruse or Kim model (eq. 2.5). For FSO links located on buildings, the acceptable height above the ground does not exceed few hundreds of meters. Thus we are most interested in low level clouds, namely Stratus, Cumulus and Stratocumulus.

Fog, haze and mist attenuation

A fog can be understood as a cloud of small water (and smoke) particles suspended into air, moving near ground. A Haze and a mist differs from a fog by visibility longer than 1km. According to the table 2.2, a fog have particle concentration of about $10 \text{ cm}^{-3} - 100 \text{ cm}^{-3}$. Thanks to presence of water droplets, a fog is significantly

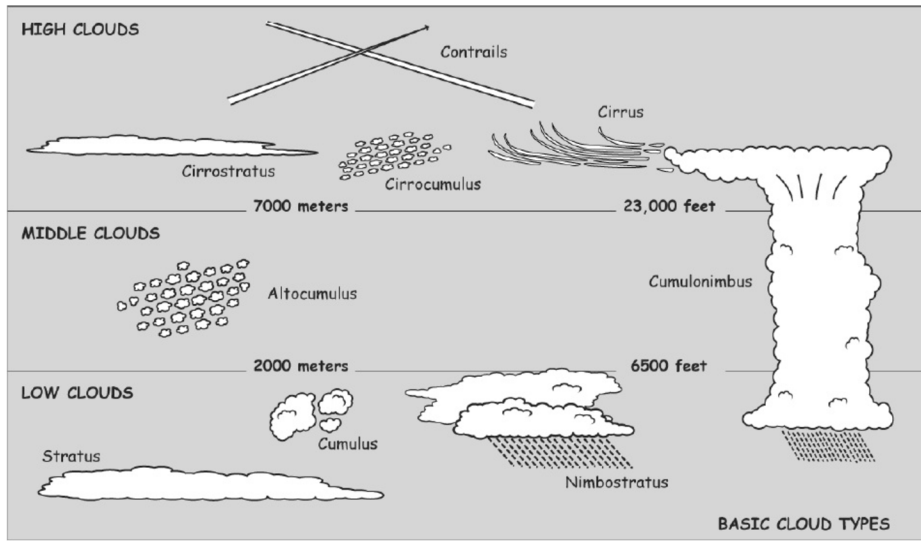


Fig. 2.3.4: Common cloud types[16]

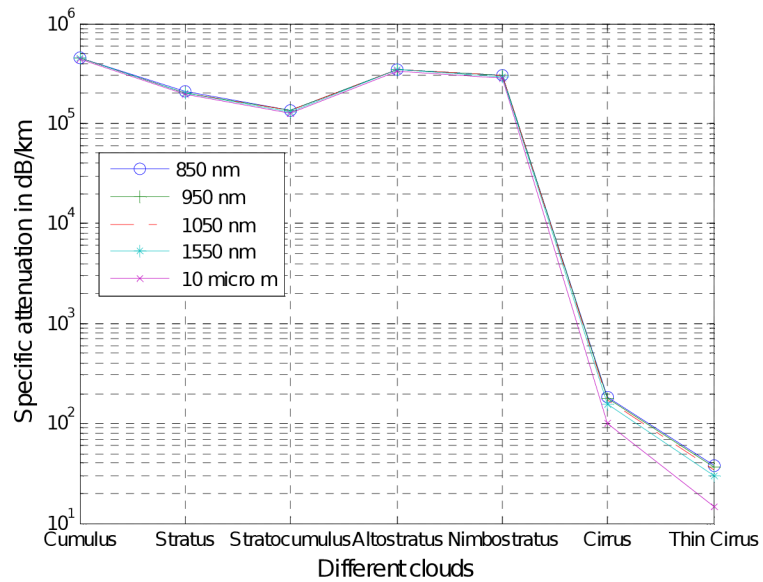


Fig. 2.3.5: Specific attenuation of different cloud types [17]

decreasing the visibility and, based on its density, causes great attenuation to an optical beam.

Two major types of a fog are distinguished, depending on how the water condensation occurred. Those differ in particle dimensions.

Radiation (continental) fog is formed by the cooling of a land after the sunset (caused by heat radiation) and its particle diameters varies around $4\mu m$. *Advection (maritime) fog* is formed when moist air passes over a cool surface by advection. An advection fog particles size are close to $20\mu m$ [18].

Based on the fact, that there is a correlation between the fog attenuation and the liquid water concentration [4], the specific attenuation coefficient (for $\lambda = 630nm$) can be expressed as:

$$\gamma = 360W^{0,64} \quad [dB/km] \quad (2.13)$$

Where W stands for liquid water concentration [kg/m^3].

The presence of a fog varies significantly over days and months and is dependent on a locality. Based on longtime measurements, a cumulative distribution probability function of a specific attenuation can be evaluated. In fig. 2.3.6, monthly variations of two month data measured at Milan at moderate continental fog conditions are shown. In this example, for 90% of the time, the specific attenuation was smaller than $10dB/km$ and for approximately 95% of time the value did not exceed $20dB/km$.

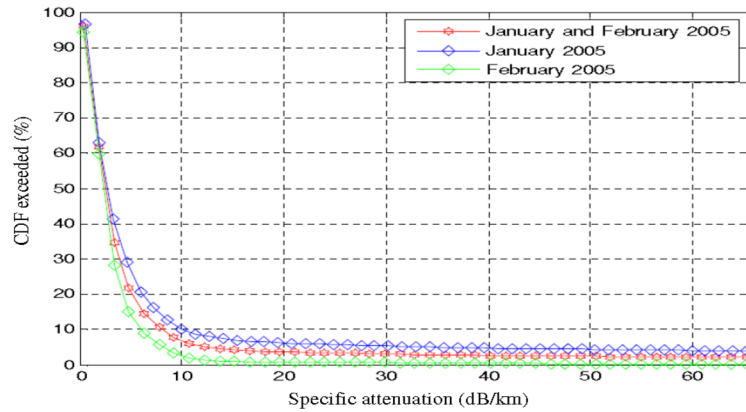


Fig. 2.3.6: Cummulative distribution function for two months[18]

The reasonable value of a link margin must be chosen based on the knowledge of a CDF function or number of days per year with fog and required link availability.

2.3.5 Precipitation attenuation

A **rain** are liquid water droplets condensed from an atmospheric vapor, heavy enough to fall due gravity. A rain attenuation is mostly caused by the scattering [4]. To evaluate the rain scattering attenuation, eq. 2.12 defined in aerosol absorption section can be used. While the used wavelength is much smaller than the particle size, the standardized cross section Q_d becomes equal to 2, wavelength independent [19]. eq. 2.12 is now simplified to:

$$\alpha_n(\lambda) = 10^5 \int_0^\infty 2\pi r^2 \frac{dN(r)}{dr} dr \quad [km^{-1}] \quad (2.14)$$

Where r and $r + dr$ means the minimal and maximal diameter of an equivalent rounded water drop and $N(r)$ is the drop size distribution. Two common drop size distribution functions are known; first of them, Marshall and Palmer (M-P) distribution function, defines the rain specific attenuation as:

$$\alpha_{rain} = 1,6 \cdot R^{0,63} \quad [dB/km] \quad (2.15)$$

The rain specific attenuation with use of Carbonneau distribution equals to [19]:

$$\alpha_{rain} = 1,076 \cdot R^{0,67} \quad [dB/km] \quad (2.16)$$

Here $R[mm/h]$ stays for the rain rate.

The graphical comparison of those models can be found in fig. 2.3.7.

Snow attenuation

A snow are flakes of frozen water, falling from clouds. Their size can reach up to 20 mm and thanks to this, fluctuations caused by snowfall can be slightly stronger than those caused by rain. A snow is classified by liquid water compound as dry or wet, having different effects on an incident beam.

A snowflake crossing laser beam can cause various attenuation, depending on the snowflake orientation, the distance from the transmitter and the cross section of the beam. A specific attenuation caused by snowfall can be expressed as [20]:

$$\alpha_{snow} = a \cdot S^b \quad [dB/km] \quad (2.17)$$

Here $S[mm/h]$ stands for a snow rate and a and b are constants, dependent on the wavelength and the snow humidity. For a wet snow:

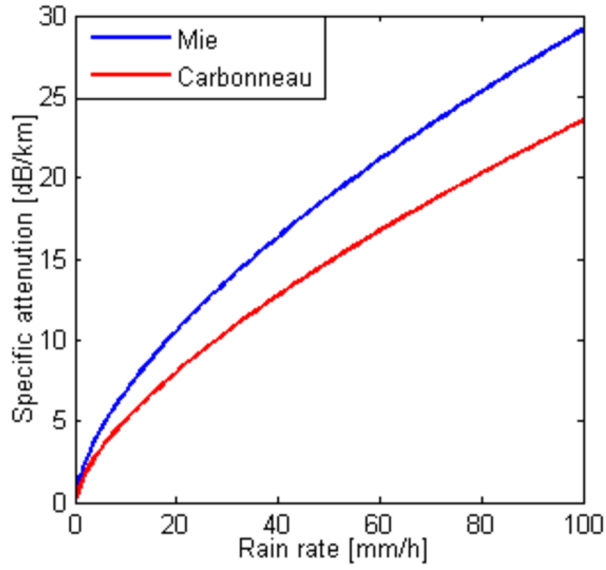


Fig. 2.3.7: Comparison of M-P and Carbonneau distributions[19]

$$a = 5,42 \cdot 10^{-5} \lambda + 5,4958776 \quad b = 1,38 \quad (2.18)$$

for a dry snow:

$$a = 1,023 \cdot 10^{-4} \lambda + 3,7855466 \quad b = 0,72 \quad (2.19)$$

From fig. 2.3.8 it is obvious, that the dependence of a specific attenuation on the snow rate is almost linear and independent on the wavelength.

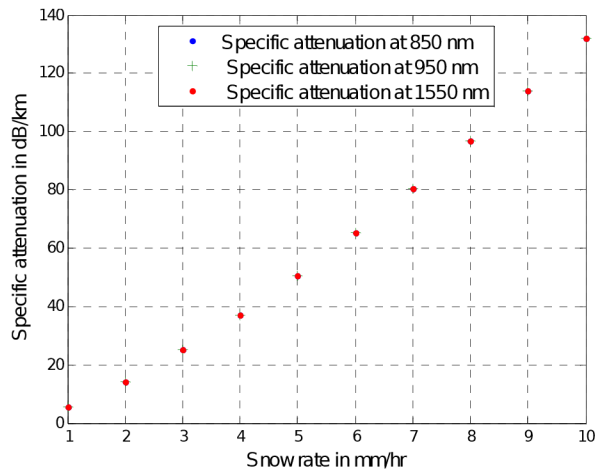


Fig. 2.3.8: Specific attenuation of a snow at different wavelengths[20]

2.4 Other phenomena

Just like the optical link, the outdoor transceiver itself is also affected by weather conditions. The further discussed outdoor transceiver is pure photonic, problems related to electronic parts (EMC, temperature range) will not be discussed.

Several phenomena which should be taken in account still remain, especially:

- Console bending caused by temperature changes of the material
- Vibrations caused by precipitation and/or wind
- A fog or a hoarfrost on the receiving optics

The first two mentioned could cause beam diversion or beam wander and are matter of transceiver case and console construction and toughness. Fogged or frozen optics cause scattering of the incident beam, leading to attenuation or extinction of the beam.

The fog on the glass is caused by adsorption of water vapour contained in air. When the air, at specific temperature and humidity blows on a solid object colder than the air, the air is being cooled and decreases its volume while the water vapour component remains. This leads to increase of relative humidity (RH). When the relative humidity reaches 100% (dew point), the air becomes saturated and additional decrease of volume (temperature) or increase of moisture causes the water to condense. The resulting beam attenuation depends on particle number and size. At temperatures below zero, the fog turns into the hoarfrost, forming small crystals of ice.

2.5 Summary

The second chapter deals with the atmosphere from a FSO point of view. An atmospheric composition and conditions are defined. Three main atmospheric phenomena affecting an optical beam - scintillations, scattering and absorption are defined and the way of predicting their presence and effect is presented. The greatest attenuation to a laser beam (hundreds of decibels) may be caused by Mie scattering (fogs), this kind of attenuation is hard to prevent differently than by sufficient power margin. On the other hand, scintillations (turbulence) cause energy fluctuations that can be avoided or at least mitigated. Atmospheric absorptions can be avoided by using suitable optical beam parameters. The construction of outdoor transmitter is equally important and should be taken in account. Next chapter presents several methods for mitigation of negative atmospheric phenomena.

3 METHODS FOR MITIGATION OF ATMOSPHERIC INFLUENCES

3.1 Aperture averaging

An aperture averaging is a common method for decreasing optical intensity fluctuations caused by turbulences at the receiver. The aperture averaging can be taken as a form of spatial diversity, because it is caused by receiving lens whose size is greater than a fading correlation width ρ_c . A receiver with an aperture size smaller than ρ_c is called a point receiver. ρ_c is obtained from a covariance function of irradiance, which describes the correlation between irradiance fluctuations at two points in the receiver plane [21]. The correlation width is defined as:

$$\rho_c = \sqrt{z/k} \quad [m] \quad (3.1)$$

Where z means the distance between the transmitter and the receiver and k is a wave number. As the aperture diameter increases above the ρ_c , low and high intensity patches incident on receiver lens get averaged, decreasing total signal fluctuations. The fading reduction, caused by aperture averaging, is quantified by an aperture averaging factor A , comparing scintillation index $\sigma_i(D)$ for the aperture diameter D and that of point receiver:

$$A = \frac{\sigma_i(D)}{\sigma_i(0)} \quad [-] \quad (3.2)$$

Increasing the aperture size have thus positive effect on the system BER. This reduction is observed at all weather conditions and turbulence strengths [22]. An example use of the aperture averaging on 3,5km long FSO link operating at wavelength of 1550nm under moderate turbulence can be seen in fig. 3.1.1.

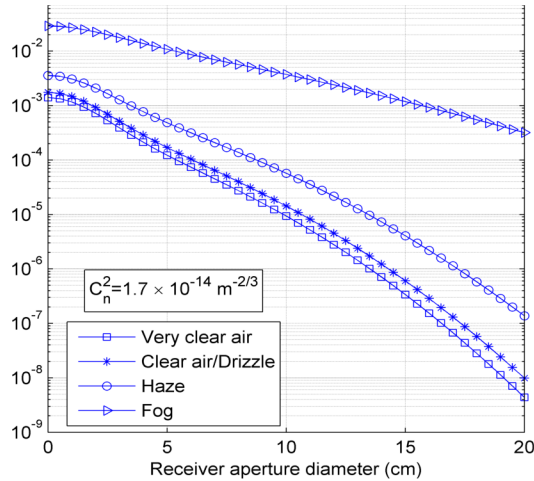


Fig. 3.1.1: BER vs. aperture diameter under various weather conditions [22]

3.2 Spatial diversity

MIMO (Multiple Input Multiple Output) is a common method of increasing the channel quality and reliability by the use of multiple spatially separated transmitters, receivers, or both mentioned.

3.2.1 Basic principle

Principle lies in splitting data into several streams, each one transmitted using own spatial channel. Multiple spatially diverged communication channels are established, those channels are thanks to variance of atmosphere parameters in space and time, affected differently, leading to application of different fading patterns on each channel. By combination of multiple received signals at receiver, resulting signal fluctuations are noticeable reduced. An example situation can be seen in fig. 3.2.1 where the effect of using 1-3 transmitters on signal fluctuations can be seen.

Different spatial diversity arrangements are distinguished:

- SISO - Single Input Single Output (no spatial diversity)
- SIMO - Single Input Multiple Output - Receiver diversity
- MISO - Multiple Input Single Output - Transmitter diversity
- MIMO - Multiple Input Multiple Output - Combination of above

To reach the mentioned effect, receivers must be sufficiently separated by a distance at least equal to the spatial coherence length L , which is defined as:

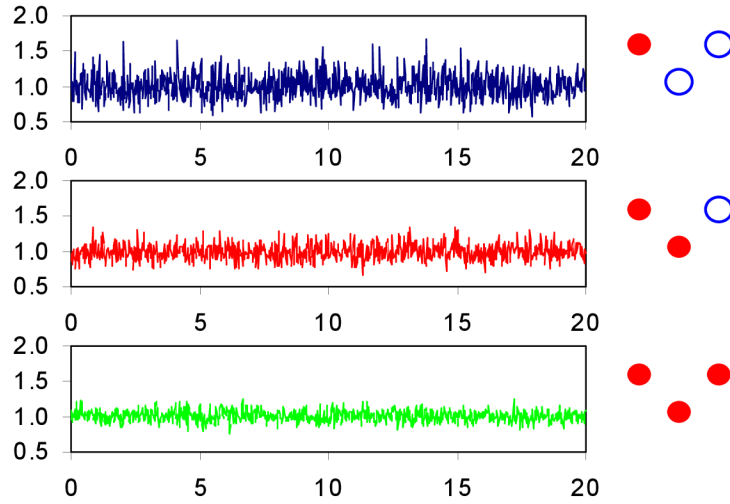


Fig. 3.2.1: Received intensity as a function of time[23]

$$L = \sqrt{\lambda z} \quad [m] \quad (3.3)$$

This assumption ensures sufficient statistical independence and uncorrelation of receiving signal [22].

3.2.2 Combining methods

Received signals are combined using one of combining techniques:

- Equal gain combining (EGC)
- Maximal ratio combining (MRC)
- Selection combining (SC)
- Threshold combining (TC)

Here *Selection combining* is continually scanning the quality of each channel and selects the channel with the best SNR. *Maximal ratio combining* sums all channels with different weights, depending on their SNR. *Threshold combining* randomly selects a channel with SNR greater than chosen threshold, if SNR falls below the threshold value, an another channel is chosen randomly. The threshold combining is simpler than the selection method [24]. *Equal gain combining* is the simplest method among them, just coherently summing all received signals. Comparison of mentioned combination methods is figured in fig. 3.2.2.

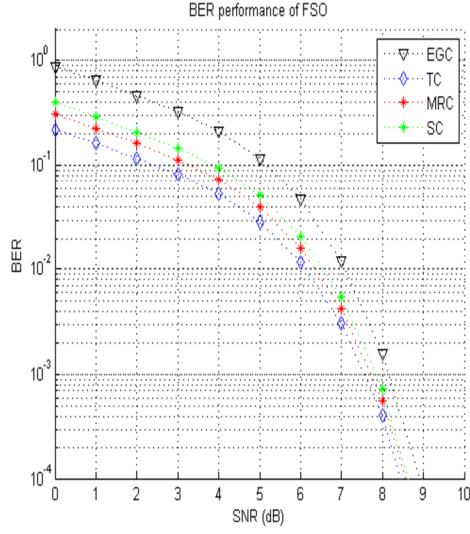


Fig. 3.2.2: Comparison of combining methods [24]

From fig. 3.2.2 it is obvious, that the best performance is reached by the use of the threshold combining, covered deeply in [24]. For further computations will be used EGC for its simplicity.

With the use of gamma-gamma distribution, resulting photocurrent from M detectors is equal to [22]:

$$i = \sum_{j=1}^M (i_{S,j} + i_{N,j}) \quad [A] \quad (3.4)$$

Where $i_{S,j}$ and $i_{N,j}$ are signal and noise contributions from j -th photodetector. Assuming that mean values and variance of signal and noise are equal, mean SNR gets increased by factor of \sqrt{M} from the value reached by single detector; scintillation coefficient gets also reduced [22]:

$$\langle SNR_M \rangle = \sqrt{2} \langle SNR_1 \rangle \quad [dB] \quad (3.5)$$

$$\sigma_{I,M}^2 = \frac{1}{M} \sigma_{I,1}^2 \quad [-] \quad (3.6)$$

In fig. 3.2.3, the dependency of the BER on the number of photodetectors under various atmospheric conditions is shown.

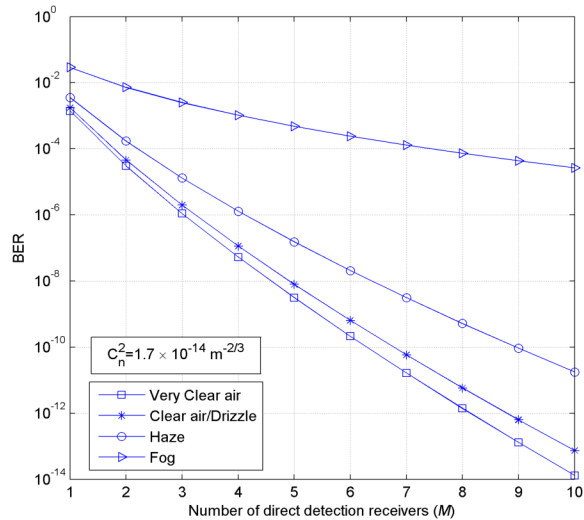


Fig. 3.2.3: BER vs the number of receivers [22]

3.2.3 Results

MIMO technology provides considerable solution for improving a channel BER (SNR) and fading. The diversity gain differs with atmospheric conditions and also depends on square root of receivers count, which (thanks to coherence length) significantly affects the transmitter size. Diversity gain is not dependent on number of transmitters [24].

3.3 Adaptive optics

Principle of the adaptive optics method lies in the prevention of long-term data losses by realtime correction of incident wavefront phase distortions. A deformable correction optical element, called *wavefront corrector* is put in front of the photodetector, compensating distortions and leading to focal plane power distribution improvement.

A part of incident beam is directed onto wavefront sensor, which detects incident wavefront distortions. Based on WFS data, the Wavefront reconstructor evaluates the need of corrector reshaping which is then translated by a control logic to the wavefront corrector (fig. 3.3.1-a). Another promising concept (model-free), is based on controlling Wavefront corrector by feedback from the photodetector (fig. 3.3.1-b).

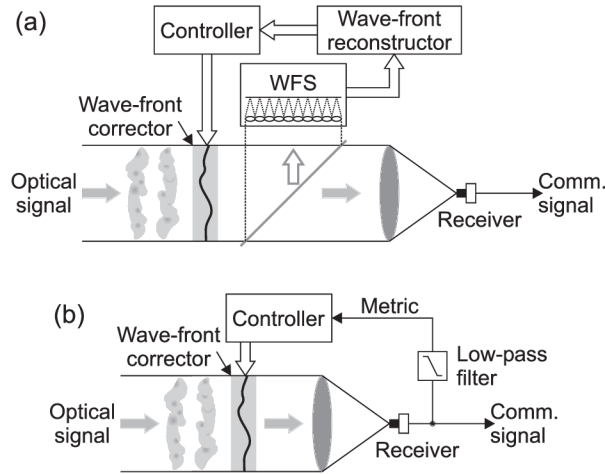


Fig. 3.3.1: Two common approaches of AO[25]

Functionality of this approach is limited only to signal captured by the receiving aperture. In order to maximize the irradiance at the receiving aperture, an adaptive transmitter system at the opposite end of the link is required [25].

An example of adaptive optics effect on the focal plane power distribution for complete wavefront correction, partial wavefront correction and no correction is shown in fig. 3.3.2.

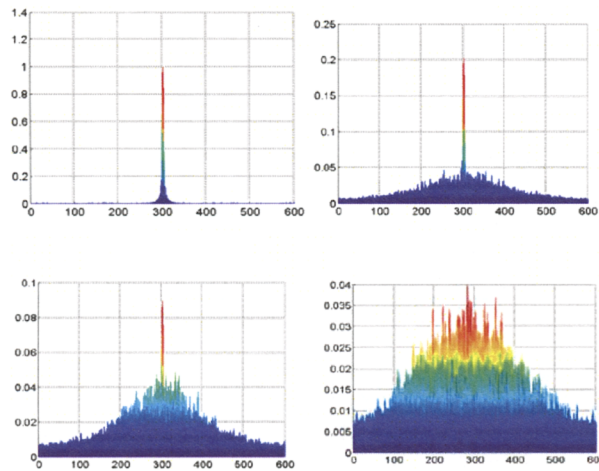


Fig. 3.3.2: Effect of AO on focal plane power distribution [26]

3.4 Channel coding and interleaving

A channel coding, also called *forward error correction* is a common method of securing a data stream against errors caused by a communication channel. The channel coding adds extra redundancy to the data stream, allowing recovery of certain amount of

erroneous bits. This principle is used in many common wireless systems such as GSM and DVB-T for years.

Channel coding allows BER improvement at constant transmitter power or transmitter power decrease at constant BER. The margin between SNR of a uncoded and a coded signal is called a coding gain and beneficially contributes to a FSO power balance. In logarithmic scale is defined as [27]:

$$G_c = 10 \cdot \log\left(\frac{E_b}{E_0}\right) - 10 \cdot \log\left(\frac{E_b}{E_0}\right)_{\text{encoded}} \quad [dB] \quad (3.7)$$

Channel codes are separated to two essential groups:

- Block codes
- Convolutional codes

3.4.1 Block codes

Block coders separate incoming data into blocks of k bits. The coding process is performed on whole block at a time. The source block of data is called a symbol, the set of all possible input symbols (bit combinations) is called a *source alphabet*.

The coding is process of assigning symbol from a source alphabet to corresponding symbol from a *code alphabet*, whose length is increased by r (redundancy). The assigning process is based on mathematical operations, whose complexity varies with used code types. On the receiver, the decoding process consists of assigning a received symbol to a symbol from code alphabet and a corresponding symbol from source alphabet. A code rate R is a measure of block code redundancy and is evaluated as a fraction of source symbol length k and an encoded symbol length n :

$$R = \frac{k}{n} \quad [-] \quad (3.8)$$

Coded symbols are independent of each other and can be transmitted and decoded separately. Common block code representatives are Hamming code, Reed-Solomon code and low-density parity check (LDPC). Block codes are qualified as (n, k) according to source and code symbol length, e.g. RS(255,239).

3.4.2 Convolutional codes

Unlike the block coding, a convolutional coding is applied continually on a data stream. The incoming data stream is being shifted bitwise into a shift register

(sliding window) of a constant length. Concurrently, at each single clock, certain logical operation is performed on a whole register, resulting with n output bits. Each encoded bit is thus dependent on other bits, whose number is determined by a shift register length. A convolutional code rate is a fraction of number of input and output bits (output logic width) [27]:

$$R = \frac{k_0}{n_0} \quad [-] \quad (3.9)$$

Common convolutional code rates are $1/2$ and $2/3$.

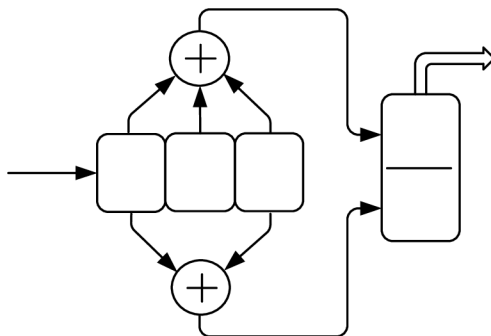


Fig. 3.4.1: An example of convolutional coder [27]

A convolutionally coded sequence can be expressed as an output sequence of a state machine with finite number of states. A graphical visualization of these states is called a *Trellis diagram*. A convolutionally coded sequence is decoded using a *Viterbi algorithm*, which determines the maximum likely path through a Trellis diagram.

Turbo codes are convolutional codes, constructed by chaining two or more particular coders together, reaching high coding gain.

Currently, the highest coding gain is reached using turbo and LDPC codes since both mentioned are almost reaching the theoretical Shannon limit. With similar coding gain, LDPC codes require noticeably lower computing power [28].

3.4.3 Interleaving

An interleaving is commonly used method of data scrambling in purpose of eliminating aggregated consecutive error bits (burst) by scattering them onto wider perspective, so that they can be better handled by channel decoder.

An interleaving is done by writing into matrix of m rows and columns while writing is performed row by row and reading by columns. An interleaver is often positioned

after a channel coder. At the opposite side of the channel, a deinterleaver with similar function is present, positioned before the channel decoder. A spreading factor is directly proportional to matrix dimensions.

An example of deinterleaving is shown in fig. 3.4.2.

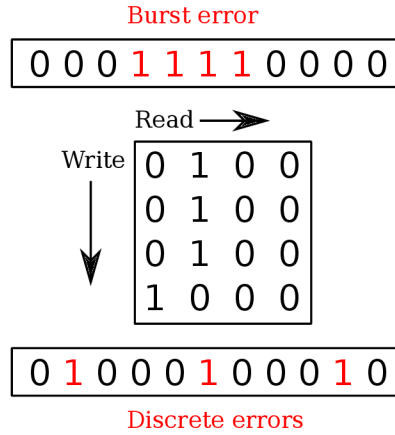


Fig. 3.4.2: Deinterleaving principle

3.5 HVAC Unit

Section 2.4 describes problems related to a water condensation on the receiving optics. The condensation can be reduced or even eliminated by reducing the relative humidity near the optics. This can be reached either by decreasing the water vapor component in air (drying the air), by increasing the volume (temperature) of air or by the combination of both methods.

The lens can either be directly heated by the electric current, flowing through resistive grid within the lens, or indirectly by the hot air from Heating, Ventilating and air Conditioning (HVAC) unit. The first mentioned method requires a special lens and provides only heating of the lens. The HVAC unit (based on its type) can maintain constant, suitable conditions either by heating during cold days or cooling during sunny days when the device is heated by the sun.

3.6 Summary

This chapter presents several methods for mitigation of negative atmospheric phenomena. The first three methods can decrease beam intensity fluctuations caused by turbulence however require intervention in the transmitter construction. Channel

coding and interleaving are methods implemented in software and can increase the power margin without any hardware modifications. The last mentioned method is addressed to effects on the FSO transceiver device itself rather than on the laser beam.

4 SUPPORT SYSTEM FOR FSO

4.1 Preface

By gathering information about link state and optical channel conditions, the atmospheric phenomena can be understood better and appropriate actions can be performed to prevent their negative influence. Following design enables both realtime and long term data gathering, their graphical representation and remote FSO transmitter management. The design is implemented on a single FPGA chip together with the Media Converter, the management is accessible via web interface. Following chapter introduces the initial design, which the support system is designated for and presents proposed system solution and top-level implementation.

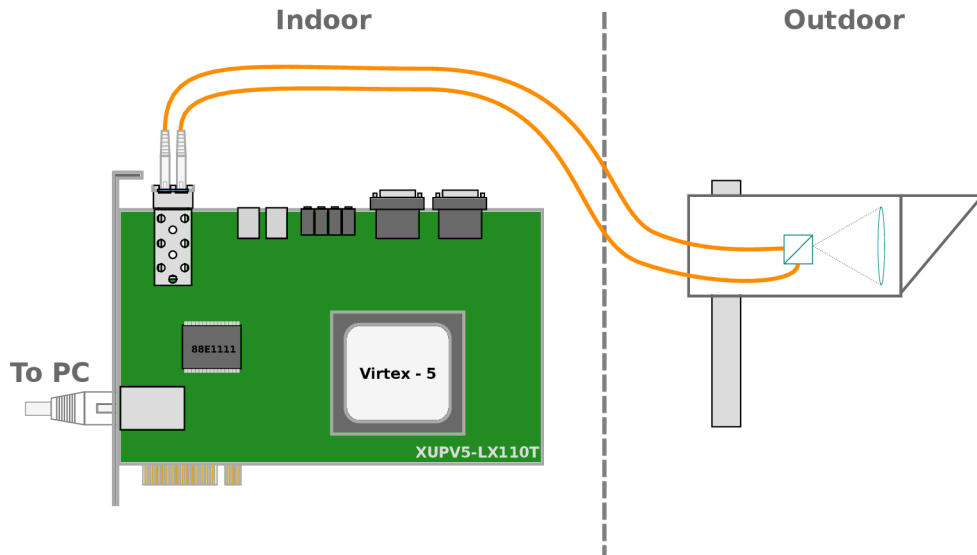


Fig. 4.1.1: Simplified system scheme

4.2 Initial design

Further discussed design is based on the working prototype of the Media Converter design implemented on the XUPV5-LX110T Evaluation Platform. The base design implements full duplex, high speed data line connecting the Ethernet PHY chip with the SFP optical transceiver, including fast fading and slow fading safeguard via Reed-Solomon (RS) encoding and frame caching, respectively. The base design works as an unmanaged media converter from metallic to optical medium and is to

be employed in an experimental FSO link. The electrical and optical frontends are split into two devices, connected by optical fibres. The fibres are linked directly to the transmitting/receiving optics.

4.2.1 XUPV5-LX110T Evaluation Platform (ML505)

The XUPV5-LX110T Evaluation Platform is Xilinx University Program unified platform for teaching and research of digital communication systems.

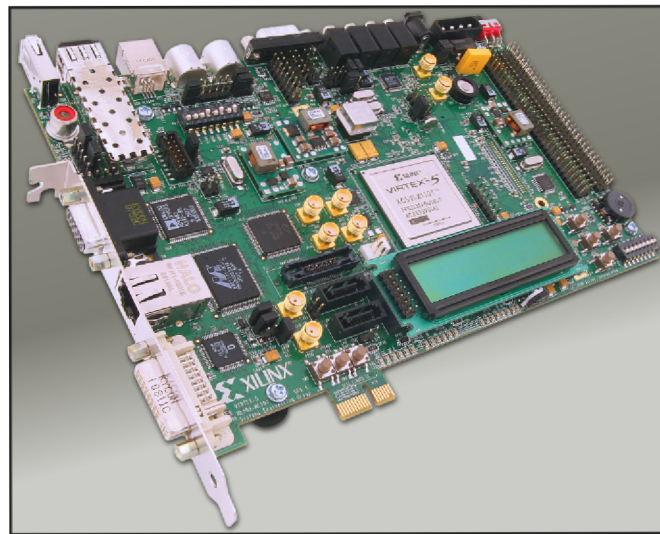


Fig. 4.2.1: XUPV5-LX110T Evaluation Platform [29]

The board is identical to ML505 Evaluation Platform, with only difference in the variant of the Virtex-5 FPGA chip - Xilinx Virtex-5 XC5VLX110T FPGA on the XUPV5 vs. XC5VLX50T on the ML505.

The Evaluation Platform contains many on-board industry standard interfaces, e.g. following :

- RJ-45 Tri-speed Ethernet PHY Transceiver
- SFP/SMA/SATA/PCI-E Gigabit transceivers
- RS-232
- USB

and memories:

- 256MB DDR2
- 32MB ZBT Flash

- 1MB SRAM
- 2x32MB Flash for device configurations
- 8Kb I^2C EEPROM

4.2.2 Media Converter

All bridged data go through the Main data line (fig. 4.2.2), which connects the Ethernet PHY chip and the SFP module.

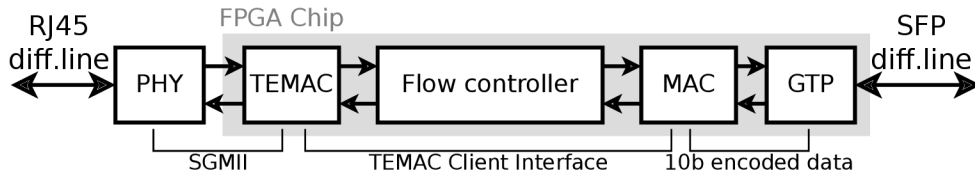


Fig. 4.2.2: Main data line block scheme with interfaces

Differential data signals from the metallic medium are processed by the onboard *PHY* chip (Marvell 88E1111) which takes care of the physical signal encoding and the conversion to serial differential SGMII interface. The PHY chip is further connected via the SGMII interface to the Xilinx *Tri-mode Ethernet Media Access Controller* (TEMAC), which is hard-wired on the FPGA and handles frame synchronization and deserialization to 8 bit wide TEMAC Client Interface. *Flow controller* acts as a frame buffer between Ethernet and SFP interfaces and passes data to the *MAC*. The MAC block handles 8b/10b conversion, RS encoding ensuring BER mitigation and a DDR FIFO for data storage during optical signal interrupts (upto about 1s). The final encoded 10 bit wide data stream is serialized in *Gigabit Transceiver* (GTP) and connected via differential pairs to the SFP module.

4.3 Proposed solution

Web servers are communicating with clients (web browsers) via TCP connections, which require implementation of the whole TCP/IP stack. A direct hardware implementation (in VHDL or verilog) of the web server and TCP/IP stack is possible however due to limited abstraction and provided functions of hardware description languages (HDL) would be very difficult and is not commonly used. For this purpose Xilinx provides softcore microcontrollers which can be customized to fit the user design. Those microcontrollers act as common single chip microcontrollers however

they are implemented within the FPGA structure. Their functionality is given by binary code compiled from assembly language or C.

PicoBlaze is a very small and simple 8-bit RISC softcore microcontroller, which can replace complex state machines and simplify the design since the program code is written in assembly language.

MicroBlaze is an advanced, 32-bit RISC softcore microcontroller. The Microblaze program code can be written in assembly or C language and compiled by GNU C Compiler (GCC). The MicroBlaze is highly configurable and is designed as a separate project in Xilinx Platform Studio (XPS). XPS allows connection of plenty further configurable IP cores to the MicroBlaze core via peripheral buses (LMB, PLB, AXI), the address space of MicroBlaze is monolithic with memory mapped I/O. The XPS project can be then either converted to the bitstream and directly loaded to the FPGA chip, or exported to the ISE project and instantiated as a black box, described by the top HDL source.

Depending on available memory (and timers), Microblaze can run a simple bare-metal firmware as well as a common Real Time Operating System (RTOS) or the Linux kernel and is thus well suitable for advanced applications including a web server. The further discussed design describes the implementation of MicroBlaze microcontroller, required peripherals and the connection to initial design. The web server is accesible from the local area network by default; if the network was connected to the internet, the device could be managed from anywhere.

4.4 Frame switching

The TCP communication between the MicroBlaze (web server) and the browser must be at some point separated from the mainstream one. Frames for MicroBlaze should be directed to its network interface and should not pass over the optical interface as well as mainstream frames should not get to MicroBlaze as they would have been dropped. The suitable place for the frame routing is Flow Controller since it is in the middle of the Main data line and disposes of the TEMAC Client interface.

4.4.1 TEMAC Client interface

TEMAC Client interface is flexible 8 bit or 16 bit wide interface designed for simplified frame handling. The client interface is further divided into two slightly different interfaces. The client receive and transmit sequences also slightly differ.

Client transmit interface

The client transmit interface defines 7 signals:

- TxCLK - Tx Clock
- TxD[7:0] - 8 bit Tx data
- TxDV - Tx Data Valid
- TxACK - Tx Acknowledge
- TxUNDERRUN
- TxCOLLISION
- TxRETRANSMIT

Last three signals will not be discussed as they are not used in the design.

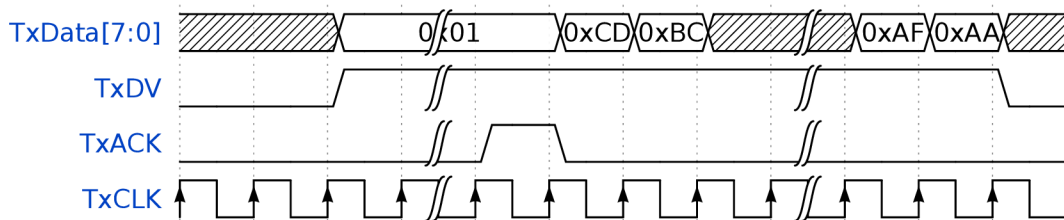


Fig. 4.4.1: TEMAC Client interface - Client transmission sequence

Transmitter sets first data byte to TxD bus and raises TxDV pin. The first byte remains on the bus until receiver acknowledges it by raising the TxACK pin. Since then, the transmitter serves new byte to TxD bus on every rising edge of TxCLK. The transmission ends by setting the TxDV signal low after the last byte. The transmission is illustrated in fig. 4.4.1

Client receive interface

The client receiver interface defines 5 signals:

- RxCLK - Rx Clock
- RxD[7:0] - 8 bit Rx data
- RxDV - Rx Data valid
- RxGF - Rx Good frame
- RxBF - Rx Bad frame

The client receiver must be ready to accept the data stream as soon as the TxDV signal is raised by the transmitter. Following bytes are loaded to the data bus with following rising edges of the RxCLK signal. The RxDV signal is set low after transmission of the last data byte. Before the next frame can be sent, either RxGF

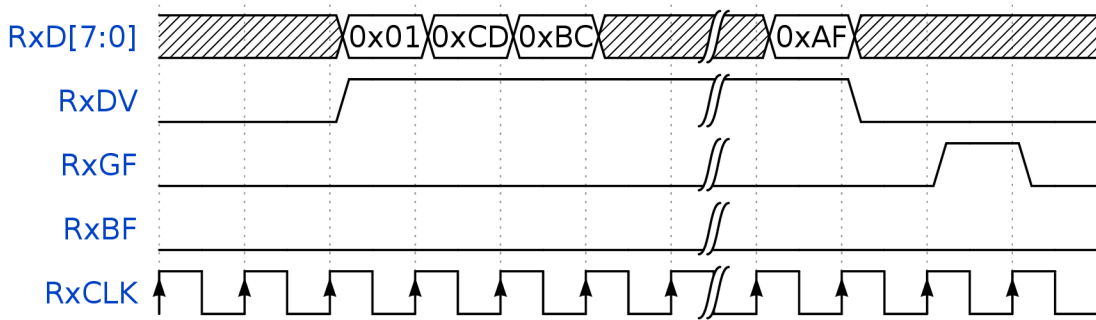


Fig. 4.4.2: TEMAC Client interface - Client reception sequence

or RxBF signal must be driven high to signalize the condition of just transmitted frame (the TxBF signal can signalize e.g. CRC mismatch). The reception sequence is illustrated in fig. 4.4.2.

4.4.2 Flow Controller

The original functionality of Flow Controller was to serve as a frame buffer between Ethernet and SFP interface. For this purpose, a single 8 bit wide FIFO memory was implemented on both data directions (fig. 4.4.3). Each FIFO is accessed by write-in (W) and read-out (R) state machines. To enable frame routing to and from Microblaze, MAC matching unit and additional two FIFOs were added. The state machines were slightly modified as well.

Frame transmission from Ethernet to SFP

Frames coming from Ethernet interface arrive to the FIFO from Ethernet to SFP interface (ETH-SFP FIFO) write-in state machine (FSM). The FSM starts writing the data to FIFO as soon as RxDV signal becomes high. This operation is clocked from the Ethernet interface and is performed independently of the SFP interface. Based on the RxBF or RxGF signal, the read-out state machine (clocked from SFP interface) either drops currently received frame (if RxBF = '1') or initializes the transmission to SFP interface by raising TxDV signal and waiting for TxACK. The interface from SFP to Ethernet is symmetric.

Frame transmission from Ethernet to MicroBlaze

In parallel with writing the data to ETH-SFP FIFO, the first six bytes of incoming frame (destination MAC address) are compared with the MAC address of MicroBlaze and the link broadcast address (FF:FF:FF:FF:FF:FF). The MAC Compare unit register is connected to the MicroBlaze core and is configurable from the software.

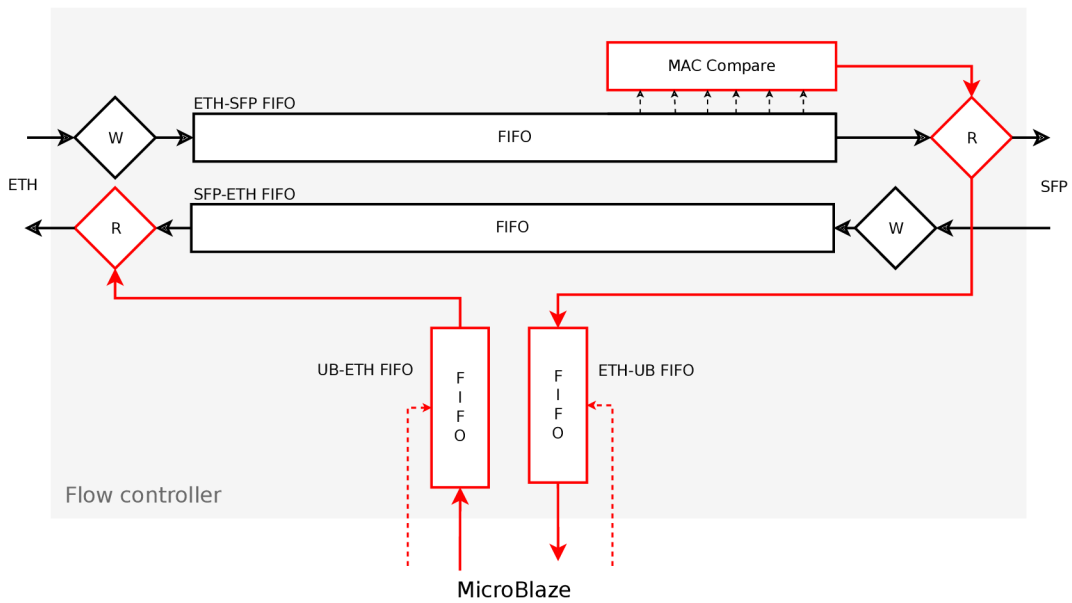


Fig. 4.4.3: Flow Controller read-out (R) and write-in (W) state machines and data FIFOs. Modified or added parts are highlighted in red.

Based on information from MAC Compare unit the SFP read-out state machine sends the frame either to SFP, MicroBlaze FIFO or both interfaces at a time.

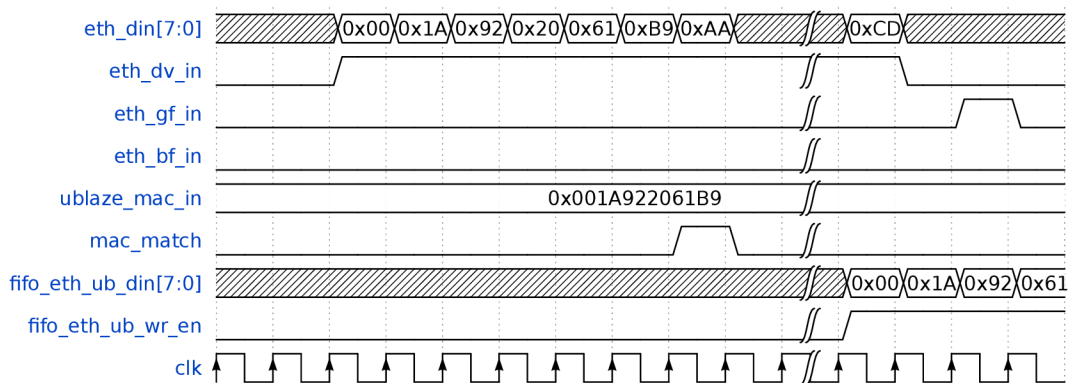


Fig. 4.4.4: Frame for MicroBlaze being processed in Flow controller

Frame transmission from MicroBlaze to Ethernet

Frames from MicroBlaze are stored in UB-ETH FIFO. The Ethernet read-out state machine starts its operation when the signal EMPTY of one of the connected FIFOs goes low. The mainline communication is prioritized since the emptiness of SFP-ETH FIFO is polled first, so the Main data line throughput is practically not affected by MicroBlaze communication. Even if there is significant traffic on mainstream, some interframe gaps occur, so the MicroBlaze takes a turn. Theoretically, when there would be so heavy traffic that frames would follow each other, the MicroBlaze would

never take a turn. To handle this situation, fixed aggregation could be applied by slight modification of the ethernet read-out state machine. A small counter could be added, limiting the maximum count of following transmissions from SFP to the Ethernet interface when the MicroBlaze Tx FIFO is not empty.

4.5 MicroBlaze design

4.5.1 Design flow

The MicroBlaze microcontroller is a very scalable modular system developed separately from HDL design in Xilinx Platform Studio (XPS). The tool allows direct generation and upload of a bitstream (standalone project). In more complex systems, the MicroBlaze design can be exported to the HDL (ISE) project as a black box described by a top HDL source defining its interface. The discussed design uses the second variant since the MicroBlaze project is a component of the Media Converter design. Following examples were created in Xilinx Platform Studio, version 14.5. - Linux, 64-bit.

Creating new XPS project

XPS provides project wizards for simple project creation. The project is characterized by peripheral bus which connects various peripherals to MicroBlaze core - AXI or PLB can be chosen. The type of peripheral bus also determines the endianness of whole MicroBlaze design (AXI is Little Endian, PLB is Big Endian). The wizard allows user to include floating point unit (FPU), to choose the size of program memory (allocated in block RAMs), to enable/disable instruction and data cache and many more. An example of composition of MicroBlaze is illustrated in fig. 4.5.1.

Adding IP cores to the design

The new design contains only a few IP cores enabling the basic functionality - the MicroBlaze core, a block RAM (BRAM) for storing the program code, BRAM controllers for connecting the BRAM to the core, a clock generator, a reset controller and a debugger. All available IP cores, which can be added to the design are listed in the IP catalog on the left side of the user interface. The catalog provides tens of categorized IP cores, e.g. :

- general purpose inputs/outputs (GPIO)
- fixed interval timers and complex, configurable timers
- bus controllers (PCI, CAN, USB, I^2C , ...)
- display drivers
- BRAM blocks
- memory controllers (SDRAM, DDR2, BRAM, EEPROM, FLASH)

The chosen IP core is appended to the *Bus interfaces* list; if the core communicates with the MicroBlaze core, it needs to be connected to the appropriate bus by expanding the IP core item in the *Bus interfaces* list and selecting the appropriate bus.

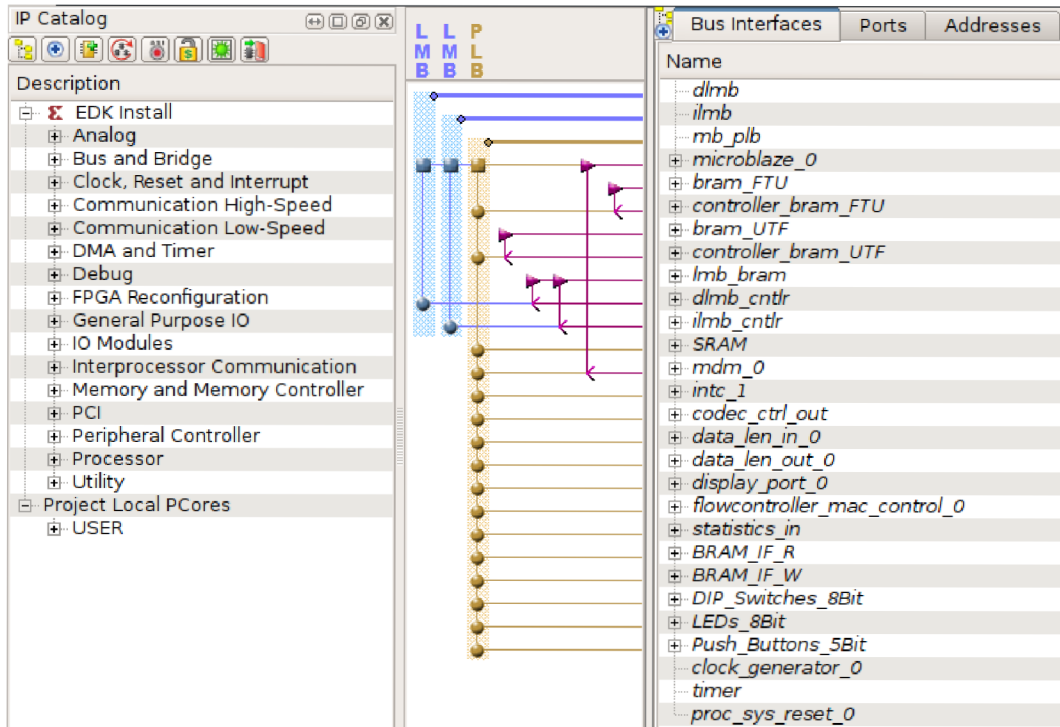


Fig. 4.5.1: XPS - Used MicroBlaze IP cores in Bus interfaces panel

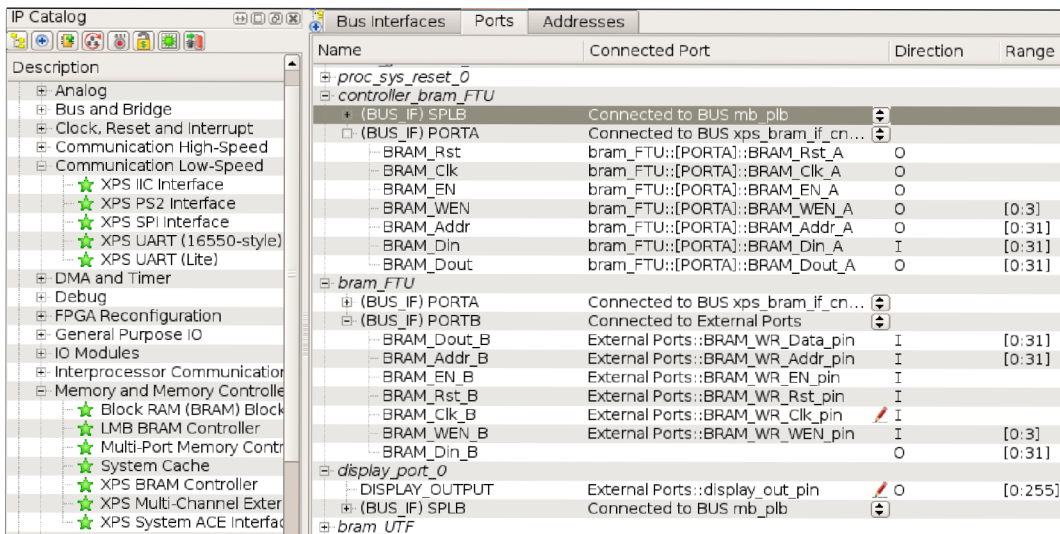


Fig. 4.5.2: XPS - IP core IO ports

The *Bus interfaces* list allows simple connection of IP cores to the MicroBlaze core however the interconnection of IP cores between each other as well as the definition of external ports is done in the *Ports* panel. The IP core list in *Ports* panel contains all IP cores added to the MicroBlaze design and their IO pins. The actual connection is done by expanding the *Connected port* menu at the desired pin or bus of the IP core and choosing the destination pin or port. The pin or port can also be connected to an external port under custom name.

In the standalone design (directly uploaded to FPGA), external ports are connected to FPGA pins and should be defined in the *ucf* file. When the design is exported to the HDL design (ISE), external ports define the interface of the MicroBlaze entity. An example situation can be seen in fig. 4.5.2. The *display_port_0* IP core's SPLB interface is connected to the MicroBlaze PLB bus, the 256 bit wide *DISPLAY_OUTPUT* port is connected via external ports to the HDL design. The *bram_FTU* IP core (BRAM block) has two interfaces, one of them (B) is provided by external ports to HDL design, the second (A) is connected via *controller_bram_FTU* (memory controller) to the MicroBlaze core. The generated MicroBlaze top HDL design would then look like the following example:

Listing 4.1: An example of MicroBlaze top HDL source

```

1  entity ublaze_top is
2    port (
3      sys_clk_pin : in  std_logic;
4      sys_rst_pin : in  std_logic;
5      ...
6      BRAM_WR_Data_pin : in  std_logic_vector(0 to 31);
7      BRAM_WR_Addr_pin : in  std_logic_vector(0 to 31);
8      BRAM_WR_EN_pin   : in  std_logic;
9      BRAM_WR_Rst_pin  : in  std_logic;
10     BRAM_WR_Clk_pin   : in  std_logic;
11     BRAM_WR_WEN_pin  : in  std_logic_vector(0 to 3);
12     display_out_pin   : out std_logic_vector(0 to 255)
13   );
14 end ublaze_top;

```

Creating custom IP cores

XPS allows creating custom IP cores described by HDL source. Those can be useful e.g. for creating special peripherals or bus interfaces. Custom IP cores are created using a wizard, which prepares a VHDL or Verilog skeleton. The custom IP core is created locally in the current project or in the global XPS repository, making it available to other XPS projects.

The IP core design typically consists of two HDL sources describing a user logic and a top level design. The user logic HDL describes the behavior of the core itself

Listing 4.2: An example of IP core user logic HDL

```
1 ...
2 entity user_logic is
3   port
4   (
5     -- Custom port
6     Ctrl_user_out  : out std_logic_vector(7 downto 0);
7     -- Interface to MicroBlaze
8     Bus2IP_Clk    : in  std_logic;
9     Bus2IP_Reset  : in  std_logic;
10    ...
11  );
12 end entity user_logic;
13
14 architecture IMP of user_logic is
15   -- Signal connected to software-accessible register
16   signal slv_reg0  : std_logic_vector(0 to C_SLV_DWIDTH-1);
17   ...
18 begin
19   ...
20   -- Connecting the custom port to software register
21   Ctrl_user_out(7 downto 0) <= slv_reg0(24 to 31);
22   -- fetch contents of software register to slv_reg0
23   SLAVE_REG_WRITE_PROC : process( Bus2IP_Clk ) is
24   begin
25     ... (generated code)
26   end process SLAVE_REG_WRITE_PROC;
27   ...
28 end IMP;
```

The top HDL source describes the interface of the IP core and instantiates and connects the user logic and the processor bus driver entities.

Address space handling

IP cores connected to the MicroBlaze core are mapped to a 32 bit monolithic address space of MicroBlaze which is handled in the *Addresses* tab. Each IP core with software registers is assigned a *Base Address* and a *High Address* from the MicroBlaze address space based on chosen size (addresses can also be assigned manually).

When exporting to SDK, the *Base Address* is exported to *xparameters.h* header file as a preprocessor macro named by *Base Name* so any change in address space is reflected in software design.

Instance	Base Name	Base Address	High Address	Size	Bus Interface	Bus Name
microblaze_0's Address Map						
dlimb_cntlr	C_BASEAD...	0x00000000	0x0001FFFF	128K	SLMB	dlimb
ilmb_cntlr	C_BASEAD...	0x00000000	0x0001FFFF	128K	SLMB	ilmb
Push_Buttons_5Bit	C_BASEAD...	0x81400000	0x8140FFFF	64K	SPLB	mb_plb
LEDs_8Bit	C_BASEAD...	0x81420000	0x8142FFFF	64K	SPLB	mb_plb
DIP_Switches_8Bit	C_BASEAD...	0x81440000	0x8144FFFF	64K	SPLB	mb_plb
BRAM_IF_W	C_BASEAD...	0x81460000	0x8146FFFF	64K	SPLB	mb_plb
BRAM_IF_R	C_BASEAD...	0x81480000	0x8148FFFF	64K	SPLB	mb_plb
intc 1	C_BASEAD...	0x81800000	0x8180FFFF	64K	SPLB	mb_plb

Fig. 4.5.3: XPS - MicroBlaze address space and IP core address mapping

4.5.2 Base design

The main purpose of MicroBlaze in the discussed design is to gather data from the Media converter design and the climatization unit and to provide the web interface representing these data and allowing control over these devices. The onboard display, leds and buttons may be advantageously used for debugging. General input/output ports are connected to the top level design via GPIO IP cores, custom IP cores are created for unidirectional ports without the interrupt support. The communication with the climatization unit is established by the XPS serial port IP core.

4.5.3 Network interface

Xilinx Platform Studio provides XPS LocalLink TEMAC core, the advanced Media Access Controller based on the hard silicon Ethernet MAC in the Virtex-5. Xilinx also provides the working port for mentioned device of LwIP, the lightweight IP stack library. The XPS LocalLink TEMAC however requires an exclusive access to the PHY chip and would take the control over the PHY chip management which is currently handled by Media Converter. Frames which should be bridged between Ethernet and SFP interface would also needed to be extracted from MicroBlaze-side interface of TEMAC (LLC bus).

In brief, the XPS LL TEMAC core provides fast and simple solution to connecting the MicroBlaze to the network in a standalone design however is hard to embed in a top level design with established mainstream connection. The development of a custom network interface for MicroBlaze will be likely more straight-forward and readable solution than creation of the wrapper for XPS LL TEMAC IP core, at the cost of porting the IP stack.

Block RAM

Xilinx Virtex-5 contains large number of 36 kb block rams (BRAM) spread in columns over the FPGA structure with total capacity of 4608 kb . The blocks have two

synchronous, symmetrical interfaces (A, B), each of them can be independently accessed. Data can be written to either or both ports and can be read from either or both ports. Each write operation is synchronous, each port has its own address, data in, data out, clock, clock enable, and write enable [30]. Block rams contain built-in FIFO support and can be cascaded to create bigger memory blocks.

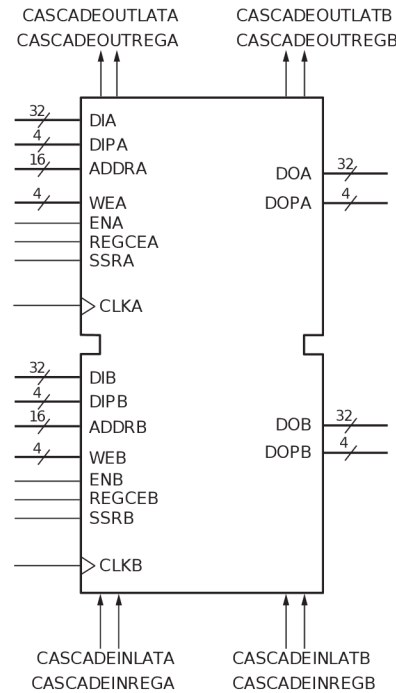


Fig. 4.5.4: Block RAM signals [30]

BRAM controller

The modified Flow Controller block stores frames for MicroBlaze in ETH - UB FIFO (see chapter 4.4.2), frames written to UB - ETH FIFO will be automatically sent to Ethernet interface. In order to process the incoming frame in the software, the frame needs to be deserialized and randomly accesible within the MicroBlaze memory space. Outgoing frames are stored as a block of data, which needs to be serialized and loaded byte-wise to UB - ETH FIFO.

Since Virtex-5 Block RAMs have two identical interfaces, they could solve both problems. They have enough space to store the frame and can be accessed randomly, with one interface wired to Flow Controller (via external ports) and the second one to the MicroBlaze. Moreover, XPS provides the *XPS BRAM Controller* IP core, which can connect the BRAM block to MicroBlaze core and map its address space into the address space of the MicroBlaze.

The *BRAM Controller* block, shown in fig. 4.5.5 is connected directly to ETH - UB and UB - ETH FIFOs of Flow Controller. When ETH - UB FIFO becomes non-empty,

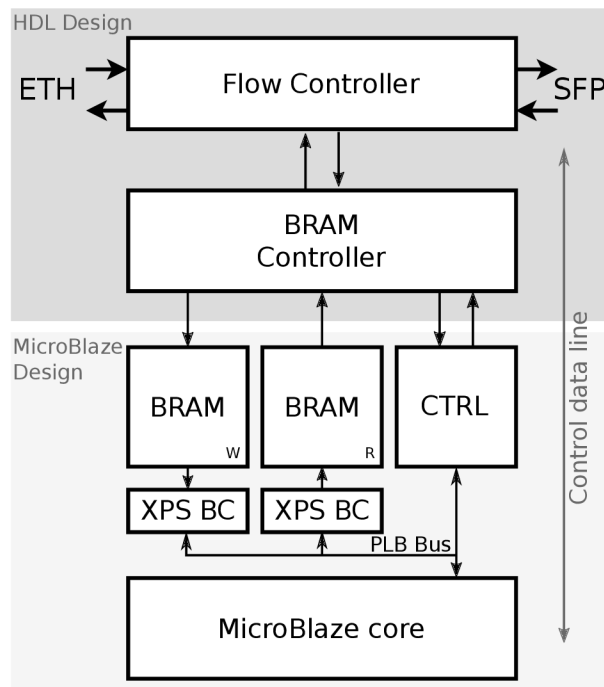


Fig. 4.5.5: Control data line - connection of MicroBlaze to Flow Controller FIFOs. XPS BC - XPS BRAM Controller IP core. CTRL - Custom IP core for control of the communication between the MicroBlaze and the BRAM controller

BRAM Controller fetches the data (single frame) to BRAM and sets the length of written data to the control interface, evoking MicroBlaze's Rx interrupt. The next frame is fetched as soon as MicroBlaze acknowledges the transmission. The MicroBlaze Tx data is fetched from the second BRAM block and written to Flow Controller as soon as MicroBlaze sets the output data length.

4.5.4 Optical path statistics

The codec contained in SFP-side MAC provides eight statistical 64 bit counters and an event FIFO. Counters are connected to the MicroBlaze core via simple read-only interface and stored as a 64 bit unsigned integer which is further provided to the web API. Provided statistical outputs are [31]:

- Total count of frames received at the SFP - side MAC
- Number of corrupted frames received at the SFP - side MAC
- Number of bytes corrected by the RS decoder
- Total number of bytes received by the receiver
- Total number of transmitted frames

- Number of output frames which had to be truncated (prematurely terminated)
- Total number of transmitted bytes
- Number of bytes dropped because of the frame buffer in SFP - side MAC overflow

The event FIFO stores up to 512 64-bit link event frames, whose format can be seen in fig. 4.5.6.

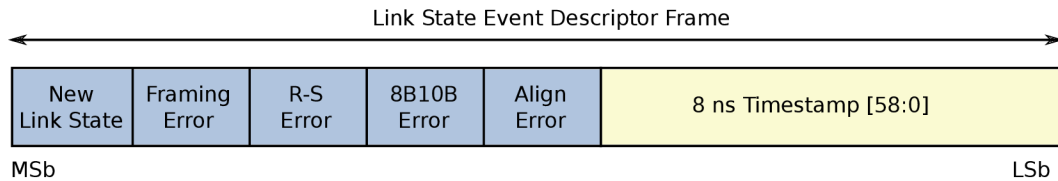


Fig. 4.5.6: Link State Frame format

The event FIFO is connected to MicroBlaze via the *stat_event_in* custom IP core. When the event count is greater than zero, the 64 bit frame is written to two 32 bit software registers, an interrupt is requested and an interrupt flag is raised in the third provided software register. As soon as the data are read and the flag is cleared, an another event can be processed.

Those events can be sent in UDP packets and visualized at host PC. Since these events are marked with timestamp, they can be advantageously visualized in a graph and the link reliability can be calculated.

4.6 Software implementation

The XPS project can be exported to Xilinx SDK which is based on Eclipse IDE. The SDK adds support for the MicroBlaze toolchain, based on GNU tools including GNU C Compiler (GCC) and GNU Project Debugger (GDB). The SDK allows the user to load the bitstream to the FPGA, to write and compile the program code, to load the binary to the program memory and to debug the code on the hardware via JTAG interface.

During the export to the SDK project, a *Hardware platform specification* project is created within the SDK. This project contains the copy of the bitstream, a bmm file describing the memory space of MicroBlaze and a xml file containing used IP cores and their parameters. From the HW platform specification project, a *Board support package* project (BSP) can be created. The BSP project is a C library providing standard C library functions and a hardware abstraction layer (HAL)

above the MicroBlaze. The HAL part of the BSP library generates the *xparameters.h* file, defining macros with base addresses, device IDs and parameters of used IP cores. The BSP also provides functions for initialization and access to MicroBlaze and connected IP cores (e.g. enabling interrupts, connecting interrupt handlers and interrupts, initialization of GPIO, access to GPIO pins, ...). The BSP project wizard also allows setting up a RTOS or Linux kernel environment, depending on the application project complexity and available resources. Following application design uses interrupt routines for handling network events and can run directly on the hardware, without an OS.

4.6.1 Software project hierarchy

The MicroBlaze SDK application project is divided into three particular parts:

- The LwIP library, defining network interface driver and providing IP stack
- The HTTP server example from LwIP contrib repository
- The main application, providing hardware abstraction, system functions and the main routine

These parts linked together with the BSP library form the final binary, uploaded to MicroBlaze.

4.6.2 LwIP

LwIP is lightweight implementation of IP stack, developed by Adam Dunkels at Swedish Institute of Computer Science [32]. LwIP is written in C and freely available and licensed under BSD-like license. The LwIP project is released as stable and is further maintained by the community. The LwIP library is designated for embedded devices with few tens of kilobytes of RAM and Flash memory. Main features are [32]:

- Protocols: IP, ICMP, UDP, TCP, IGMP, ARP, PPPoS, PPPoE
- DHCP client, DNS client, AutoIP/APIPA (Zeroconf), SNMP agent (private MIB support)
- APIs: specialized APIs for enhanced performance, optional Berkeley-like socket API
- Extended features: IP forwarding over multiple network interfaces, TCP congestion control, RTT estimation and fast recovery/fast retransmit

- Addon applications: HTTP server, SNMP client, SMTP client, ping, NetBIOS nameserver
- Experimental support for IPv6

These features can be enabled or disabled by preprocessor macros defined in lwipopts.h. LwIP can run either standalone or on underlying operating system. For non-os applications, LwIP provides low-level *raw API* (callback API), running in single execution context (thread). High-level (sequential) APIs should run in its own thread and thus require an OS. High-level *Netconn API* and *Socket API* are provided. The second mentioned is very similar to POSIX socket API, applications using the Socket API are thus easily portable to other operating systems, e.g. Linux. This project uses the raw API since it provides the best performance.

Porting LwIP to custom network interface

To use LwIP with a custom hardware, low-level functions of LwIP must be reimplemented. User must provide functions to initialize the network interface, to send and receive a frame and to get the system time. The *lwip/netif/ethernetif.c* file within the LwIP root is a skeleton providing templates for these functions.

Listing 4.3: ethernetif.c: Prototypes of elementary LwIP functions

```

1 static void low_level_init(struct netif *netif);
2 static err_t low_level_output(struct netif *netif, struct pbuf *p);
3 static struct pbuf *low_level_input(struct netif *netif);

```

Especially for TCP timeouts, LwIP requires access to the system time via `sys_now()`; function. This function returns the actual value of 32 bit unsigned integer variable which gets incremented every 10 ms by the fixed interval timer, the timer period must also be defined in lwipopts.h.

The frame transmission happens transparently within LwIP however for frame reception, the `ethernet_input()` function must be called after fetching a new frame to the BRAM. After meeting these requirements, the LwIP can be initialized and used.

LwIP Initialization

The LwIP is initialized in three steps:

Listing 4.4: LwIP initialization

```

1 void lwip_init(void);
2 struct netif *netif_add(struct netif *netif, ip_addr_t *ipaddr,
3                       ip_addr_t *netmask, ip_addr_t *gw,
4                       void *state, netif_init_fn init,
5                       netif_input_fn input);
6 void netif_set_up(struct netif *netif);

```

The `lwip_init()` function initializes built-in LwIP modules (memory, statistics, UDP, TCP, ...) and takes no parameters. After module initialization, the network interface is initialized and added to the interface list by `netif_add()` function. The network interface is assigned the IP address, subnet mask, default gateway and init and input callback functions. The network interface is enabled by calling `netif_set_up()`. The `check_timeouts()` function should be called periodically from main loop to check LwIP timers.

Since now, the IP stack is initialized; if ARP and ICMP are not disabled in `lwipopts.h`, the application should respond to ICMP echo requests (fig. 4.6.1).

SRC	DEST	PROT	
aa:bb:cc:dd:ee:ff	Broadcast	ARP	60 Gratuitous ARP for 192.168.1.16 (Request)
192.168.1.13	192.168.1.16	ICMP	98 Echo (ping) request id=0x3a48, seq=1/256
aa:bb:cc:dd:ee:ff	Broadcast	ARP	60 Who has 192.168.1.13? Tell 192.168.1.16
AsustekC_de:df:a8	aa:bb:cc:dd:ee:ff	ARP	42 192.168.1.13 is at bc:ae:c5:de:df:a8
192.168.1.16	192.168.1.13	ICMP	98 Echo (ping) reply id=0x3a48, seq=1/256

Fig. 4.6.1: An example of ARP and ICMP communication between PC (192.168.1.13) and LwIP at MicroBlaze (192.168.1.16)

4.6.3 HTTP server

A HTTP server is an application, responding to HTTP requests of a client (browser). Typically, the client sends the HTTP GET request to the server (with information about the client and the path to the requested page) and the server responds by sending the HTTP header (with information about server) and the requested page.

The LwIP repository contains a simple HTTP server example. The server has dependency on LwIP and works just after simple initialization by calling `httpd_init()` function. Since most lightweight applications do not provide common filesystem functionality, the HTTP server provides a virtual filesystem stored in the program code memory. The HTTP root folder must be converted into bit arrays, which are then included and passed to the HTTP GET handler. The conversion is done by `makefsdata` script. The script processes files in “fs” subdirectory and creates a `fsdata.c` file containing single array of type `unsigned char` for each file.

SSI Module

By default, the HTTP server allows only a static HTML presentation. The response of the server contains a HTTP server header and contents of the requested page which was pre-generated by `makefsdata` utility and is a part of the program code. To include data dynamically provided during the application runtime, an additional functionality is required. For this purpose, the HTTP server example provides a

Server-Side Include (SSI) module which can be enabled in `httpd.h` file. This module looks for special tags in the source webpage (which is generated the same way as before) and appends the generated string right after the tags. The tag is within the HTML comment, which remains in the code but since it is a comment, it does not affect the visible content. The tag has following syntax:

```
<!--#name-->
```

The application should provide an array of tag names and the function returning strings based on given tags.

Listing 4.5: `httpd.h`: Prototypes of SSI functions

```
1 typedef u16_t (*tSSIHandler)(int iIndex, char *pcInsert, int iInsertLen);
2 void http_set_ssi_handler(tSSIHandler pfnSSIHandler,
3                          const char **ppcTags, int iNumTags);
```

This allows web server to pass data from the main routine to the webpage, e.g. the frame/byte counters from the top level design can be now inserted into a simple web page. In the fig. 4.6.2, the very first version of the web interface utilizing only ssi can be seen.

FSO Statistics

Parameter	Value
RX_FRAMES_RECEIVED	1
RX_FRAMES_BAD	0
RX_BYTES_CORRECTED	0
RX_BYTES_RECEIVED	60
TX_FRAMES_SENT	1
TX_FRAMES_TRUNCATED	0
TX_BYTES_SENT	60
TX_BYTES_DROPPED	0
UB_FRAMES_SENT	12
UB_FRAMES_RECEIVED	28

©2016 DREL FEEC BUT

Fig. 4.6.2: The first version of simple web interface with top level counters. Only SSI used.

CGI Module

To enable the backward communication from a browser to a web server, the server provides the Common Gateway Interface (CGI) module. When the webpage with `.cgi` extension is requested, the CGI module looks for a CGI handler which is associated to

the requested filename. If the handler is found, it is called with data from the browser as parameters. This allows sending data from web forms or javascript variables to the main application. In this project, the CGI engine is used e.g. for enabling or disabling the channel encoding or for setting the climate control unit.

Listing 4.6: httpd.h: Prototypes of CGI functions

```

1 typedef const char *(*tCGIHandler)(int iIndex , int iNumParams, in
2                                     char *pcParam [], char *pcValue []);
3 void http_set_cgi_handlers(const tCGI *pCGIs, int iNumHandlers);

```

The CGI engine is initialized by calling *http_set_cgi_handlers()* with pointer to *tCGI struct* and total number of handlers as parameters. The *tCGI struct* encapsulates the CGI handler-filename string pair.

The webdesign

The final webdesign is inspired by Network Gateway project [33]. The design is divided into tabs, each containing single category. The design is formed by CSS and simple javascript framework handling tabs and buttons. Statistical data or current settings are passed to the page by the SSI engine.

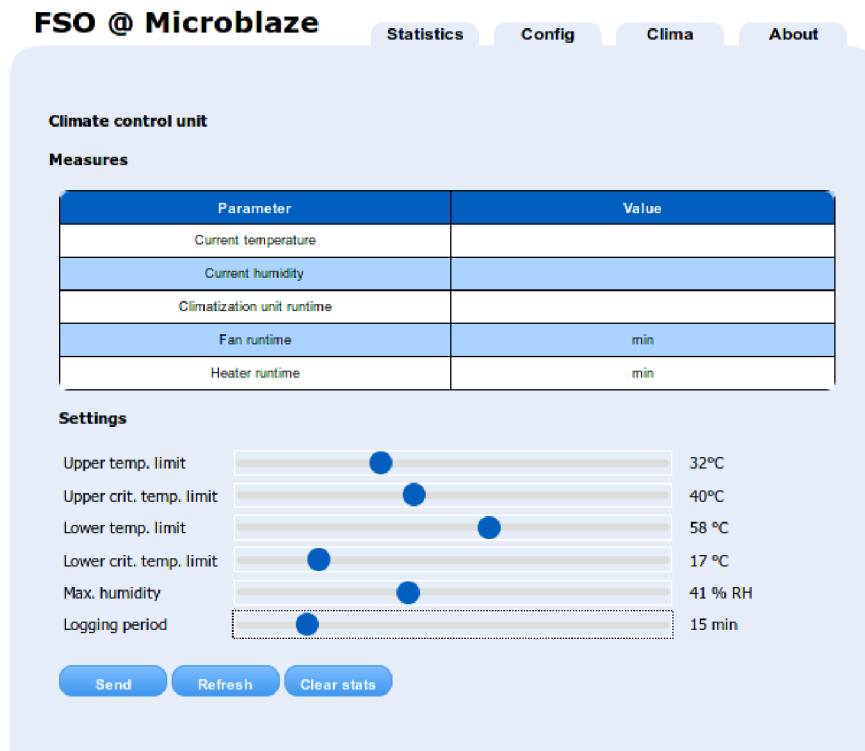


Fig. 4.6.3: Current version of web interface

By clicking submit buttons (FSO config. or Clima config.), the data from forms are sent by HTTP GET method to appropriate CGI handler.

4.7 Climate control unit

This design utilizes a simple HVAC unit [34], attached to the outdoor FSO transceiver. The unit is powered by a 48V power supply and is designated to prevent the optics from dew or freezing, to maintain suitable temperature conditions within the transceiver device and to provide temperature and humidity information.

4.7.1 Provided functionality

The HVAC unit provides a simple interface and is connected to the host (Media Converter design) via serial bus. The unit is fully automatized and its operation is driven by following software controllable limit values:

Tab. 4.1: Software controllable temperature and humidity limits

Value	Unit	Meaning
t_h	°C	upper temperature limit
t_{h_krit}	°C	upper critical temperature limit
t_d	°C	lower tempereture limit
t_{d_krit}	°C	lower critical temperature limit
h_{max}	% RH	humidity limit

The HVAC unit contains temperature and humidity sensors

Cooling process

When the ambient temperature reaches the upper temperature limit t_h , the fan starts to operate. The fan speed is linearly increasing from the minimal to the maximal value, depending on the ambient temperature. The fan reaches its maximal speed when the ambient temperature reaches t_{h_krit} .

Heating process

The heating process starts when the ambient temperature reaches the lower temperature limit t_d or the humidity reaches the maximum humidity limit h_{max} . The heater and the fan are triggered and the duty cycle of the heater is linearly regulated by the ambient temperature. The maximum duty cycle is set when the ambient temperature reaches the lower critical temperature limit t_{d_krit} .

4.7.2 RS-485 Driver

The HVAC unit is connected to the Evaluation Platform via RS-485 bus. Since the Evaluation Platform does not provide a RS-485 driver, a simple reduction from UART to RS-485 must be constructed. A Texas Instruments SN65HVD10D was used as an all-in-one driver with only few external resistors, a blocking capacitor and transient voltage suppressors. The schematics is in fig. 4.7.1

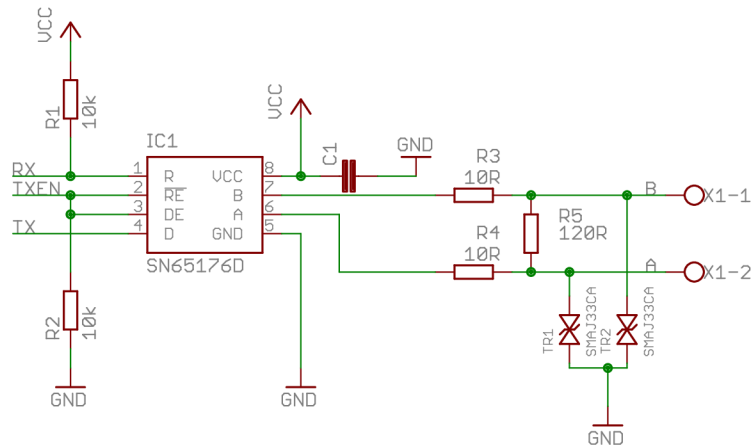


Fig. 4.7.1: Schema of the RS-485 driver board

The bus driver is to be mounted directly on the XUPV5 board to headers *J5* and *J6*.

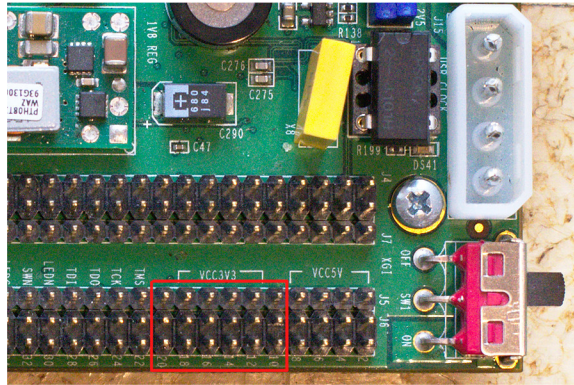


Fig. 4.7.2: Positioning of the RS-485 driver on pinheaders *J5* and *J6*

For detailed documentation of the RS-485 driver board, see appendix C.1.

4.7.3 Serial interface

Microblaze communicates with the HVAC unit at 9600 b/s with no parity. In the MicroBlaze design, a common XPS UART Lite IP core is used and wired to Tx

and Rx pins of the RS-485 driver. The TxEN pin is handled from software. The software registers of the device are then accessed by simple get/set instructions, e.g. "D10" command sets the t_{d_krit} to 10°C. Those commands are handled from the Microblaze based on requests from the web GUI.

4.7.4 Proposed improvements

Operation of the discussed HVAC unit is triggered when the ambient temperature or the humidity reaches preset limits. This works fine for keeping the transceiver temperature in service limits of used parts. The dew however could occur even if the air temperature rises much faster than the temperature of the optics, the increased humidity also does not always cause a fogging. This could be prevented by setting loose values of temperature and humidity limits, at the cost of increased unnecessary fan and heater runtime.

Decreasing the run time of a HVAC

The condensation of the water vapour on a solid surface can be well predicted by calculating the dew point temperature T_{dp} . A dew point is the temperature, at which air, as a result of isobaric cooling, becomes saturated without supplying additional vapour [35]. The dew point can be calculated from air temperature T [°C] and a relative humidity V [%RH] using following empiric equation from NOAA [36]:

$$T_{dp} = \frac{243.5 \ln \left(\frac{V}{100} e^{\frac{17.67 \cdot T}{243.5 + T}} \right)}{17.67 - \ln \left(\frac{V}{100} e^{\frac{17.67 \cdot T}{243.5 + T}} \right)} \quad [^{\circ}C] \quad (4.1)$$

By periodic calculation of the dew point, based on data from the temperature and humidity sensor, the anti-fogging mechanism could operate only when there is an actual risk of fogging.

Air drying

By increasing the temperature of the optics, the risk of fogging is mitigated. While the water condensation depends either on air temperature and moisture, the anti-fogging mechanism would be even more effective when the air was also dehumidified.

The use of peltier element could theoretically solve either dehumidification and heating of the air. By blowing the air on the cold side of the peltier element (much colder than the optics), the excessive vapour condenses on the surface of the peltier element. The cold, dry air could then be heated by the hot side of the peltier element. See appendix C.3 for a theoretical example of the method.

4.8 Summary

This chapter discusses the implementation of the support system for FSO bridge, based on the MicroBlaze microcontroller. To connect the MicroBlaze core to the network, a custom simple ethernet switch and a custom network interface was designed. The LwIP library, providing IP functionality, was ported to the design. An example HTTP server from the same repository was used to provide HTTP functionality. A graphical web interface was designed to provide remote control over the whole system and the connected HVAC unit. This chapter also briefly describes functionality of the HVAC unit and the design of a simple RS-485-UART converter board.

CONCLUSION

In the first, theoretical, part of the thesis, a FSO link is introduced and its components are discussed with mention of requirements. An atmosphere is explained, with focus on atmospheric phenomena affecting the FSO link. Each phenomenon has different matter and possibility of prediction. Their effect on propagating beam can be more or less mitigated or even avoided by suitable methods. The crucial problem is caused by Mie scattering of aerosols (fog), the attenuation can reach even several hundreds of decibels and can be mitigated by a sufficient power margin of the FSO link. By the use of an appropriate beam wavelength, the atmosphere absorption can be neglected. The remaining phenomenon - scintillations, caused by turbulences and leading to beam wandering, can be successfully mitigated by several methods which are explained in the third chapter.

The second, practical, part of the thesis deals with the design and the realization of a support system for a FSO link. The whole design is based on the unmanaged Media Converter design, implemented on a single FPGA chip of Xilinx XUPV5 Evaluation Platform. A softcore microcontroller MicroBlaze is implemented on the top level HDL design as the core of the support system. A custom network switch and network interface was implemented to connect the MicroBlaze to the Ethernet network. An IP stack functionality is provided by custom port of LwIP library. The MicroBlaze runs web server, providing interactive user interface, that allows user to remotely control all parameters provided by the top level design and the connected HVAC unit. The remote user gets full control over connected HVAC unit and provided top level design (vid. appendix B). Based on settings from the web interface, the microcontroller sends UDP packets with link events - e.g. when the optical beam is interrupted or when the frame synchronization is lost. Those packets contain a timestamp and thus could be harvested and visualized in remote PC.

The support system allows user to remotely control the system, the user also gains access to information about long-term and short-term link reliability, bit error rate and weather and link conditions. Those data can then be involved in studies of the optical channel.

The git repository of the thesis, including the text, the ISE project, the XPS project and the software project is available at: <https://gitlab.com/OK2NMZ/thesis-fso>.

BIBLIOGRAPHY

- [1] Claude Chappe. *Wikipedia: the free encyclopedia* [online]. [cited 12 December 2015]. Available from: https://en.wikipedia.org/wiki/Claude_Chappe
- [2] MAJUMDAR, Arun K. *Free-space laser communication performance in the atmospheric channel* [online]. 2005. [cited 9 December 2015]. Available from: <http://link.springer.com/10.1007/s10297-005-0054-0>
- [3] Stimulated Emission. *Wikipedia the free encyclopedia* [online]. [cited 16 December 2015]. Available from: https://en.wikipedia.org/wiki/Stimulated_emission
- [4] BOUCHET, Olivier. *Free-space optics: propagation and communication*. Newport Beach, 2006. ISBN 9781905209026.
- [5] CAPLAN, David O. *Laser communication transmitter and receiver design* [online]. 2007. [cited 9 December 2015]. Available from: <http://link.springer.com/10.1007/s10297-006-0079-z>
- [6] WILFERT, Otakar. *Kvantová a laserová elektronika*. Brno: Brno university of technology, 2012. ISBN 978-80-214-4493-5.
- [7] Pin-Diode. *Wikipedia: die freie Enzyklopädie* [online]. 2001. [cited 10 December 2015]. Available from: <https://de.wikipedia.org/wiki/Pin-Diode>
- [8] POON, Andrew. Lecture 12: Photodiode Detectors. *Advanced Photonics Technologies* [online]. [cited 10 December 2015]. Available from: <http://course.ee.ust.hk/elec509/>
- [9] WILFERT, Otakar. *Optoelektronika*. Brno: Brno university of technology, 2002.
- [10] ALKHOLIDI, Abdulsalam Ghalib and ALTOWIJ, Khaleel Saeed. *Free Space Optical Communications — Theory and Practices* [online]. 2014. [cited 10 December 2015]. ISBN 978-953-51-1732-2. Available from: <http://www.intechopen.com/books/contemporary-issues-in-wireless-communications/free-space-optical-communications-theory-and-practices>
- [11] Fog. *Wikipedia: the free encyclopedia* [online]. 2001. [cited 11 December 2015]. Available from: <https://en.wikipedia.org/wiki/Fog>
- [12] RAMMPRASATH, K. and PRINCE, Shanthi. *Analyzing the cloud attenuation on the performance of free space optical communication* [online]. 2013.

- [cited 11 December 2015]. ISBN 978-1-4673-4866-9. Available from:
<http://ieeexplore.ieee.org/lpdocs/epic03/wrapper.htm?arnumber=6577165>
- [13] IJAZ, M., GHASSEMLOOY, Z., LE-MINH, H., PEREZ, J., PESEK, J. and FISER, O. *Experimental validation of fog models for FSO under laboratory controlled conditions* [online]. 2013. [cited 11 December 2015]. Available from:
<http://ieeexplore.ieee.org/lpdocs/epic03/wrapper.htm?arnumber=6666097>
- [14] KŘIVÁK, P. *Optické bezkabelové spoje s velkým dosahem*. Brno: Brno University of Technology, 2009.
- [15] Spectroscopy of Rocks and Minerals, and Principles of Spectroscopy. [online]. [cited 16 December 2015]. Available from:
<http://speclab.cr.usgs.gov/PAPERS.refl-mrs/refl4.html>
- [16] LAZARRO. *Skywatchers and Clouds*. [online]. [cited 11 December 2015]. Available from: <http://www.epubbud.com/read.php?g=YYGRJMN3>
- [17] NADEEM, F., LEITGEB, E. and KANDUS, G. *Comparing The Cloud Effects on Hybrid Network Using Optical Wireless and GHz Links* [online]. 2010. [cited 12 December 2015]. Available from:
<http://ieeexplore.ieee.org/xpl/articleDetails.jsp?arnumber=5580354>
- [18] AWAN, Muhamad Saleem, LEITGEB, Erich, KHAN, Muhamad Saeed, NADEEM, Farukh and CAPSONI, Carlo. *Evaluation of fog attenuation results for optical wireless links in free space* [online]. 2008. [cited 11 December 2015]. ISBN 978-1-4244-1947-0. Available from:
<http://ieeexplore.ieee.org/lpdocs/epic03/wrapper.htm?arnumber=4656761>
- [19] BRÁZDA, Vladimír, SCHEJBAL, Vladimír and FIŠER, Ondřej. *Rain impact on FSO link attenuation based on theory and measurement* [online]. 2012. [cited 11 December 2015]. ISBN 978-1-4577-0920-3. Available from:
<http://ieeexplore.ieee.org/lpdocs/epic03/wrapper.htm?arnumber=6206120>
- [20] NADEEM, F., LEITGEB, E., AWAN, M. S. and KANDUS, G. *Comparing the snow effects on hybrid network using optical Wireless and GHz links* [online]. 2009. [cited 11 December 2015]. Available from:
<http://ieeexplore.ieee.org/lpdocs/epic03/wrapper.htm?arnumber=5286388>
- [21] VISWANATH, Anjitha, JAIN, V. K. and KAR, Subrat. *Experimental evaluation of the effect of aperture averaging technique on the performance of free space optical communication link for different intensity modulation schemes* [online]. 2015. [cited 12 December 2015]. Available from:
<http://ieeexplore.ieee.org/lpdocs/epic03/wrapper.htm?arnumber=7098679>
- [22] KAUR, Prabhmandeep, JAIN, Virander Kumar and KAR, Subrat. *BER*

- performance improvement of FSO links with aperture averaging and receiver diversity technique under various atmospheric conditions* [online]. 2014. [cited 12 December 2015]. Available from:
<http://ieeexplore.ieee.org/lpdocs/epic03/wrapper.htm?arnumber=7036552>
- [23] KOREVAAR, Eric, KIM, Isaac I. and MCARTHUR, Bruce. *Atmospheric Propagation Characteristics of Highest Importance to Commercial Free Space Optics* [online]. [cited 20 April 2016]. Available from:
<http://laseritc.com/files/files/MRV-WP-FSOAtmosProp.pdf>
- [24] JOHNSI, A. Arokiamarie and SAMINADAN, V. *Performance of diversity combining techniques for FSO-MIMO system* [online]. 2013. [cited 12 December 2015]. Available from:
<http://ieeexplore.ieee.org/lpdocs/epic03/wrapper.htm?arnumber=6577100>
- [25] WEYRAUCH, Thomas and VORONTSOV, Mikhail A. *Free-space laser communications with adaptive optics: Atmospheric compensation experiment* [online]. 2004. [cited 13 December 2015]. Available from:
<http://link.springer.com/10.1007/s10297-005-0033-5>
- [26] HASHMI, A., EFTEKHAR, A., YEGNANARAYANAN, S. and ADIBI, A. *Analysis of optimal Adaptive Optics system for Hybrid RF-wireless optical communication for maximum efficiency and reliability* [online]. 2008. [cited 13 December 2015]. Available from:
<http://ieeexplore.ieee.org/lpdocs/epic03/wrapper.htm?arnumber=4777475>
- [27] PROKEŠ, Aleš. *Rádiové komunikační systémy*. Brno: Brno University of Technology, 2013.
- [28] KHAN, Ahmad and ROY, K. *Comparison of Turbo Codes and Low Density Parity Check Codes* [online]. 2013. [cited 13 December 2015]. Available from:
<http://iosrjournals.org/iosr-jece/papers/Vol6-Issue6/C0661118.pdf>
- [29] Xilinx University Program XUPV5-LX110T Development System. [online]. [cited 11 April 2016]. Available from:
<http://www.xilinx.com/univ/xupv5-lx110t.htm>
- [30] Virtex-5 FPGA User Guide. [online]. [cited 20 April 2016]. Available from:
http://www.xilinx.com/support/documentation/user_guides/ug190.pdf
- [31] NOVÁK, Marek. *FSO transceiver for link quality estimation*. Brno: Brno University of Technology, 2016.
- [32] LwIP - A Lightweight TCP/IP Stack. [online]. [cited 20 April 2016]. Available

from: <http://savannah.nongnu.org/projects/lwip/>

[33] NOVÁK, Marek. Network Gateway. [online]. [cited 29 April 2016]. Available from: <https://gitlab.com/OK2NMZ/NGW>

[34] JANOŠÍK, T. *Klimatizační jednotka do optické hlavice*. Brno: Brno University of Technology, 2013.

[35] DVOŘÁK, Petr. *Zlepšení metod předpovědi termické konvekce pro účely letecké meteorologie*. Praha: Univerzita Karlova v Praze, 2009.

[36] Wet-Bulb Temperature and Dewpoint Temperature from Air Temperature and Relative Humidity. [online]. [cited 21 April 2016]. Available from: <http://www.srh.noaa.gov/images/epz/wxcalc/wetBulbTdFromRh.pdf>

LIST OF SYMBOLS, PHYSICAL CONSTANTS AND ABBREVIATIONS

FSO Optical system with free space communication channel – Free Space Optics

WiFi Name for IEEE 802.11b standard – Wireless Fidelity

RF Electromagnetic wave frequency in the range from 3kHz to 300GHz – Radio Frequency

PTP Communication between two points (single transmitter, single receiver) – Point To Point

BER Number of transmitted error bits per total number of transmitted bits at defined time – Bit Error Ratio

SNR The ratio between signal and noise power level – Signal to Noise Ratio

RVR The distance at which an airplane pilot can see runway landing marks. Similar to visibility – Runway Visual Range

MOR The distance at which optical beam intensity is reduced to 5% of its previous value – Meteorological Optical Range

MIMO Method of spatial divergence where multiple transmitters and receivers are used – Multiple Input Multiple Output

ROF Fog present in real situation rather than model – Real Outdoor Fog

CDF The function that describes probability of variable to reach particular values – Cumulative Distribution Function

DSD The function of raindrop size distribution – Drop Size Distribution

AO Method of decreasing longtime signal fluctuations by optical element shaping – Adaptive Optics

WFS Device for measuring wavefront distortion – Wavefront Sensor

FEC Channel coding method with possibility of fixing limited number of erroneous bits – Forward Error Correction

FPGA Digital circuits containing programmable logical blocks interconnected by programmable matrix – Field Programmable Gate Array

SFP System of interchangeable network modules – Small Form Pluggable

VHSIC U.S. Government research program from 1980. – Very High Speed Integrated Circuit

VHDL Hardware description language for describing digital and mixed-signal integrated circuits and field programmable gate arrays – VHSIC hardware Description Language

XPS Development tool for MicroBlaze system – Xilinx Platform Studio

MAC Link layer device (Layer II. of ISO/OSI model) – Media Access Controller

FIFO Method of manipulating with memory buffer – First In, First Out

IDE Complex application for software development – Integrated Development Environment

SDK A set of tools for software development – Software Development Kit

API Programming interface of some application or library – Application Programming Interface

POSIX Family of programming standards for compatibility of operating systems – Portable Operating System Interface

HTTP Protocol for HTML presentation exchange – HyperText Transfer Protocol

SSI Technique of replacing special html tags with data generated by web server – Server-Side Includes

CGI Protocol for passing messages from web browser to external scripts – Common Gateway Interface

HVAC Air conditioning system – Heating, Ventillating and air Conditioning unit

LIST OF APPENDICES

A MicroBlaze project	71
B Web UI	73
C HVAC	75

A MICROBLAZE PROJECT

Tab. A.1: Used IP cores (generic)

Name	Description
dlmb	Local Memory Bus controller (data)
ilmb	Local Memory Bus controller (instructions)
mb_plb	Processor Local Bus controller (master)
microblaze_0	MicroBlaze core
lmb_bram	BRAM block for the program
bram_FTU	BRAM block (Flowcontroller to Microblaze)
bram_UTF	BRAM block (Microblaze to Flowcontroller)
dlmb_cntlr	Memory controller (data)
ilmb_cntlr	Memory controller (instructions)
controller_bram_FTU	Memory controller (FTU block)
controller_bram_UTF	Memory controller (UTF block)
SRAM	Memory controller (onboard SRAM)
mdm_0	MicroBlaze Debug Module
intc_1	Interrupt controller
BRAM_IF_R	Interface to BRAM Controller - input
BRAM_IF_W	Interface to BRAM Controller - output
DIP_switches_8bit	DIP switches interface
LEDS_8bit	LED signalization interface
Push_Buttons_5bit	Push buttons interface
serial_port	UART interface to HVAC unit
clock_generator_0	Clock generator
timer	Fixed interval timer for systick
proc_sys_reset_0	Procesor system reset module

Tab. A.2: Used IP cores (custom)

Name	Description
config_interface_0	Configuration and control IF (resets, etc.)
data_len_in_0	Data length from BRAM controller
data_len_out_0	Data length to BRAM controller
display_port_0	Paralel display interface
flowcontroller_mac_control_0	MAC address output for FlowController

Name	Description
stat_events	Statistics - Event interface
statistics_input_0	Statistics - Counter interface

B WEB UI

FSO @ Microblaze Statistics Config Clima About

FSO link statistics

Parameter	Value
RX_FRAMES_RECEIVED	
RX_FRAMES_BAD	
RX_FRAMES_BAD / RX_FRAMES_RECEIVED	< NaN
RX_BYTES_CORRECTED	
RX_BYTES_RECEIVED	
TX_FRAMES_SENT	
TX_FRAMES_TRUNCATED	
TX_BYTES_SENT	
TX_BYTES_DROPPED	
UB_FRAMES_SENT	
UB_FRAMES_RECEIVED	

Refresh

Fig. B.0.1: Web UI - Statistics

FSO @ Microblaze Statistics Config Clima About

FSO link configuration

Channel Coding: Disabled ▾

BER Simulator: Disabled ▾

BER Value: None ▾

Event Frame Broadcast: Enabled ▾

Send Refresh

Fig. B.0.2: Web UI - Configuration

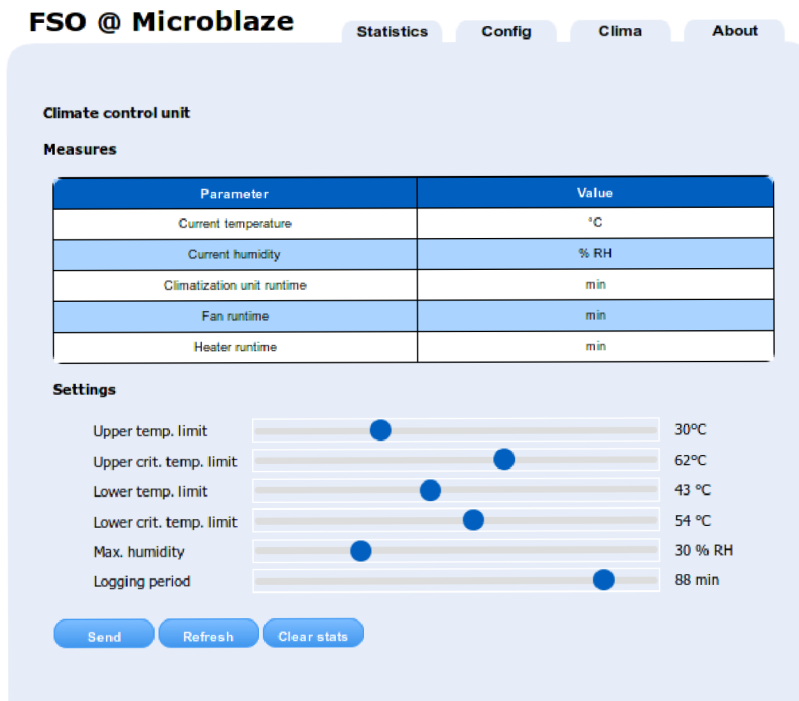


Fig. B.0.3: Web UI - HVAC configuration



Fig. B.0.4: Web UI - About

C HVAC

C.1 Driver board

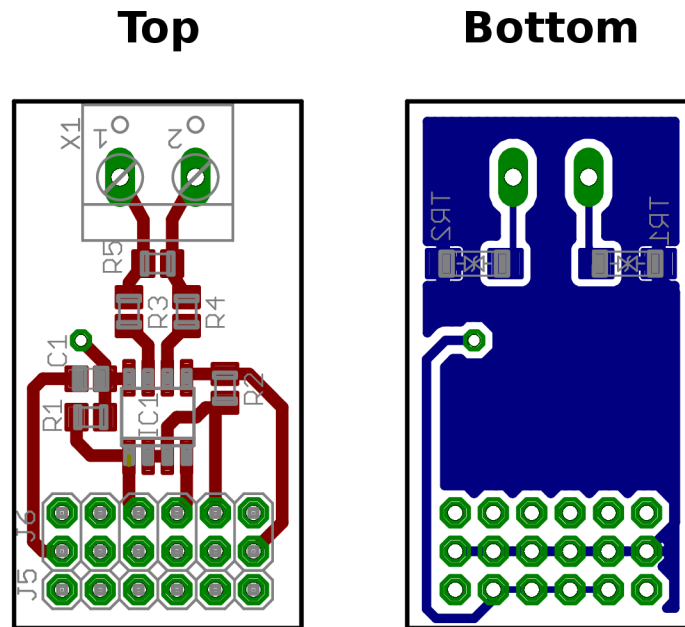


Fig. C.1.1: RS-485 Driver board - Assembly, scale 2:1

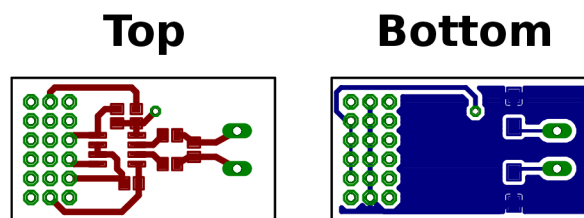


Fig. C.1.2: RS-485 Driver board - Layout, scale 1:1

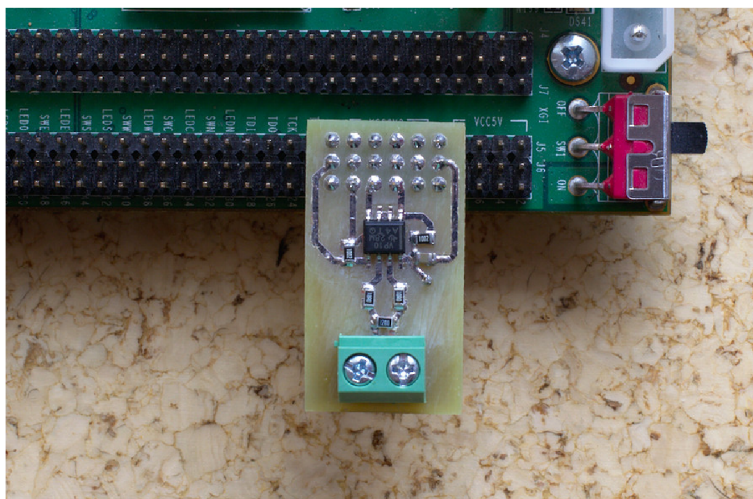


Fig. C.1.3: Assembled RS-485 Driver board

Tab. C.1: RS-485 Driver board partlist

Caption	Part	Value	Footprint
R1	Resistor	10 $k\Omega$	0805
R2	Resistor	10 $k\Omega$	0805
R3	Resistor	10 Ω	0805
R4	Resistor	10 Ω	0805
R5	Resistor	120 Ω	0805
C1	Ceramic capacitor	100 nF	0805
TR1	Bipolar TVS	6V, 600 W	SMB
TR2	Bipolar TVS	6V, 600 W	SMB
IC1	RS-485 Driver	SN65176D	SOIC-8
J5	Pinheader	1 \times 6, 2.54 mm	-
J6	Pinheader	2 \times 6, 2.54 mm	-
X1	Terminal bar	1 \times 2,5 mm	-

C.2 HVAC Unit commands

Tab. C.2: HVAC command list

Command	Description	Range	Example
m	Print the menu	-	m
t	Get the current temperature	-	t
h	Get the current humidity	-	h
p	Get EEPROM contents	-	p
n	Reset service counters	-	n
o	Repair done	-	o
r	Get current limits	-	r
Hxx	Set the t_h	0-99 °C	H40
Kxx	Set the t_{h_krit}	0-99 °C	K50
Dxx	Set the t_d	0-99 °C	D10
Lxx	Set the t_{d_krit}	0-99 °C	L5
Vxx	Set the h_{max}	10-90 %RH	V70
Zxx	Set the log period	0-99 min ¹	Z10
Ixx	Set the minimal heating current	0-99 ²	I10

¹When set to 0, the writing period will be 10s.

²Actual current is calculated by multiplying the register value by 10 [mA]. e.g. I10 sets the current to 100 mA.

C.3 HVAC Improvements

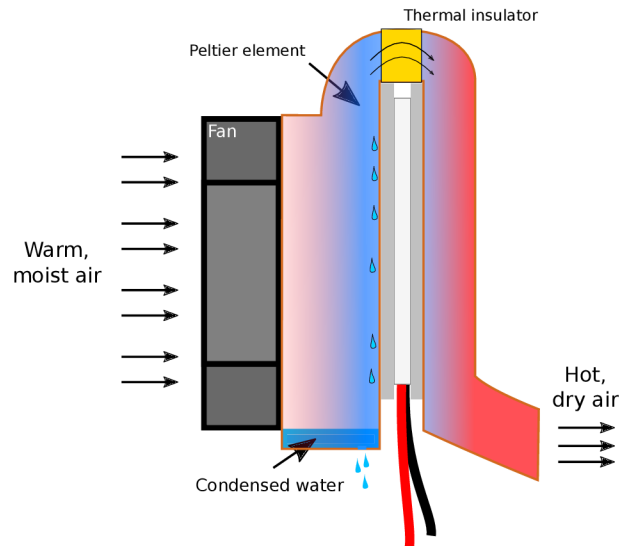


Fig. C.3.1: Theoretical construction of HVAC with Peltier element